

See discussions, stats, and author profiles for this publication at: <https://www.researchgate.net/publication/305269402>

Vigorous deep-sea currents cause global anomaly in sediment accumulation in the Southern Ocean

Article in *Geology* · July 2016

DOI: 10.1130/G38143.1

CITATIONS

7

READS

939

4 authors, including:



Dietmar Müller

The University of Sydney

475 PUBLICATIONS 23,167 CITATIONS

SEE PROFILE

Some of the authors of this publication are also working on these related projects:



Application of data science in mineral exploration [View project](#)



AUGURY [View project](#)

Vigorous deep-sea currents cause global anomaly in sediment accumulation in the Southern Ocean

Adriana Dutkiewicz¹, R. Dietmar Müller¹, Andrew McC. Hogg^{2,3}, and Paul Spence^{3,4}

¹EarthByte Group, School of Geosciences, University of Sydney, Sydney, NSW 2006, Australia

²Research School of Earth Sciences, Australian National University, Canberra, ACT 0200, Australia

³ARC Centre of Excellence for Climate System Science, University of New South Wales, Sydney, NSW 2052, Australia

⁴Climate Change Research Centre, University of New South Wales, Sydney, NSW 2052, Australia

ABSTRACT

The vigorous current systems in the Southern Ocean play a key role in regulating the Earth's oceans and climate, with the record of long-term environmental change mostly contained in deep-sea sediments. However, the well-established occurrence of widespread regional disconformities in the abyssal plains of the Southern Ocean attests to extensive erosion of deep-sea sediments during the Quaternary. We show that a wide belt of rapid sedimentation rates (>5.5 cm/k.y.) along the Southeast Indian Ridge (SEIR) is a global anomaly and occurs in a region of low surface productivity bounded by two major disconformity fields associated with the Kerguelen Plateau to the east and the Macquarie Ridge to the west. Our high-resolution numerical ocean circulation model shows that the disconformity fields occur in regions of intense bottom-current activity where current speeds reach 0.2 m/s and are favorable for generating intense nepheloid layers. These layers are transported toward and along the SEIR to regions where bottom-current velocities drop to <0.03 m/s and fine particles settle out of suspension, consistent with focusing factors significantly greater than 1. We suggest that the anomalous accumulation of sediment along an 8000-km-long segment of the SEIR represents a giant succession of contourite drifts that is a major extension of the much smaller contourite east of Kerguelen Plateau and has occurred since 3–5 Ma based on the age of the oldest crust underlying the deposit. These inferred contourite drifts provide exceptionally valuable drilling targets for high-resolution climatic investigations of the Southern Ocean.

INTRODUCTION

The palimpsest nature of the abyssal seafloor is nowhere more apparent than in the Southern Ocean where the mighty Antarctic Circumpolar Current (Fig. 1), comprising a series of braided jets, transports a massive volume of ocean water eastward at an estimated $137 \pm 7 \times 10^6 \text{ m}^3/\text{s}$ (Meredith et al., 2011). Pioneering magnetostratigraphic analysis of deep-sea sediment cores (Goodell and Watkins, 1968; Kennett and Watkins, 1976; Ledbetter and Ciesielski, 1986; Osborn et al., 1983; Watkins and Kennett, 1972) provided an unprecedented view of the dynamic nature of deep-sea currents in the Southern Ocean and their deleterious effect on the continuity of the sedimentary record. This evidence was supported by direct observations of ocean-bottom bedforms (Kennett and Watkins, 1976; Kolla et al., 1976) and manganese nodules (Watkins and Kennett, 1977).

Understanding the transport of modern deep-sea sediment is critical for accurate models of paleoclimate and the widespread use of the sedimentological record as a proxy for productivity where the connection between the seafloor and sea surface is controvertible. The Southern Ocean, where diatoms contribute ~75% of

primary production (Crosta et al., 2005) and dominate biogenic sediments (Goodell et al., 1973), is a case in point. However, most of the key studies on large-scale sediment reworking in the Southern Ocean were conducted when relatively little was known about the oceanography of this region, and even the bathymetry and tectonic fabric, which underpin the distribution of deep-sea currents, were lacking detail. Here we combine a high-resolution numerical model of bottom currents with sedimentological data to constrain the redistribution of sediment across the abyssal plains and adjacent mid-ocean ridges in the Southern Ocean.

METHODOLOGY

The distribution of Holocene disconformities is based on our compilation of data on cored surface sediments sampled in the Southern Ocean that are missing material younger than 11.7 ka. The data set includes a total of 632 sites with paleomagnetic and/or micropaleontologic ages from USNS *Eltanin* piston cores (Kennett and Watkins, 1976; Osborn et al., 1983; Watkins and Kennett, 1972) and ARA *Islas Orcadas* cores (Ledbetter and Ciesielski, 1986), and 302 sites where the surface sediment has been radiocarbon

dated, is constrained by an age model, or is demonstrably undisturbed (Geibert et al., 2005). The latter includes the Chase and Burckle (2015) compilation and additional sites from various cruises (see the GSA Data Repository¹).

Long-term average sedimentation rates (Fig. 1A; Fig. DR1 in the Data Repository) were calculated using global sediment thickness (Whitaker et al., 2013; Fig. DR2) and crustal age (Müller et al., 2016; Fig. DR3). For 63 sites, we obtained age model-derived sedimentation rates and focusing factors (ψ) given as the ratio of sediment accumulation rate to ²³⁰Th-normalized sediment flux (vertical sediment rain rate) (Dezileau et al., 2000; Francois et al., 2004; see the Data Repository and Table DR1). Regions with sediment focusing have $\psi > 1$, and those with sediment winnowing have $\psi < 1$ (Dezileau et al., 2000; Francois et al., 2004).

We use the global ocean-sea ice model (Geophysical Fluid Dynamics Laboratory [GFDL] Modular Ocean Model version 1 [MOM1], <http://mom-ocean.org>) to simulate global ocean circulation at a resolution that results in realistic velocities throughout the water column and is ideal for estimating interaction between time-dependent bottom currents and ocean bathymetry. The model is based on the GFDL CM2.6 fully coupled climate model (Griffies et al., 2015). GFDL-MOM1 nominally has a 1/10° horizontal resolution, has 50 vertical levels, and resolves mesoscale variability over the majority of the global ocean (see Griffies et al., 2015, their figure 1). GFDL-MOM1 is equilibrated for 35 yr with repeated CORE Normal Year atmospheric Forcing (CORE-NYF) (Griffies et al., 2009).

SEDIMENTATION RATES AND FOCUSING FACTORS

Long-term average sedimentation rates in the global ocean have a median value of 0.5 cm/k.y. (Fig. DR1). Rates of 6–10 cm/k.y. with

¹GSA Data Repository item 2016216, description of sedimentological datasets, Table DR1, and Figures DR1–DR20, is available online at www.geosociety.org/pubs/ft2016.htm, or on request from editing@geosociety.org.

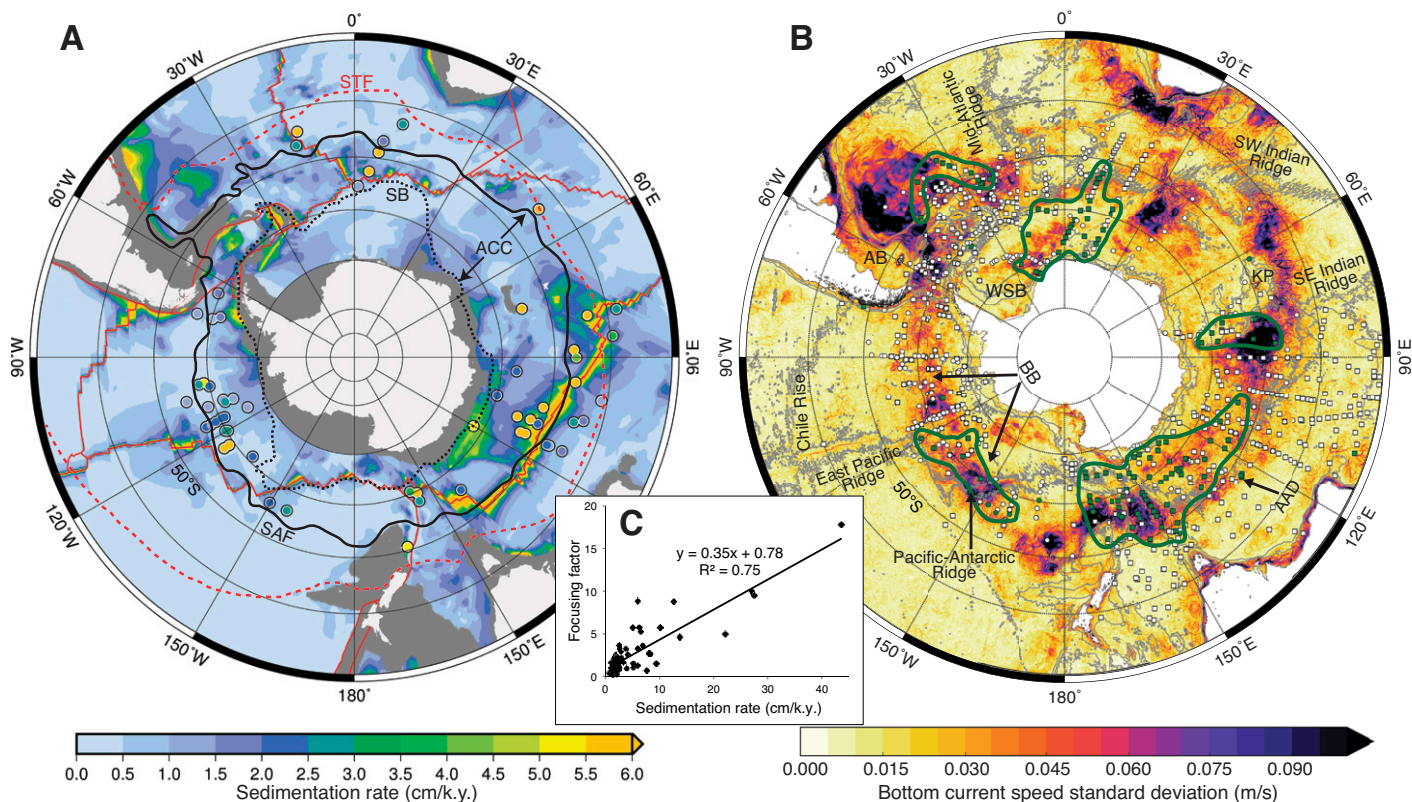


Figure 1. Sedimentation rates versus bottom current speeds in Southern Ocean. Stereographic projection. A: Long-term average sedimentation rates overlain with Holocene age model–derived sedimentation rates (Table DR1 [see footnote 1]). Contours from Carter et al. (2009): Subtropical Front (STF, dashed red line), Subantarctic Front (SAF, solid black line), Southern Boundary (SB, dashed black line) of Antarctic Circumpolar Current (ACC). Solid red lines denote plate boundaries. **B:** Standard deviation of modeled present-day bottom-current speeds, which is more representative than mean values because Southern Ocean experiences large variations in bottom-current speed. Conformities (white symbols) and unconformities (green symbols) in Holocene sediment are shown as squares when based on magnetostratigraphic data and as circles in all other cases (see text and the Data Repository for details). Major unconformity fields are highlighted by green outlines. KP—Kerguelen Plateau; AAD—Australian–Antarctic discordance; AB—Argentine Basin; WSB—Weddell Sea Basin; BB—Bellingshausen Basin. Note that maximum depth of AB (6.2 km) exceeds depth in our model (5.5 km), resulting in truncation of topography needed to dissipate flow. WSB is outside of influence of ACC and its discordance field is largely the product of ice streams creating powerful erosive turbidity currents (Huang and Jokat, 2016) not captured in our model. **C:** Focusing factors versus Holocene sedimentation rates for Southern Ocean (see the Data Repository and Table DR1 therein).

maxima >50 cm/k.y. occur near continental margins and are prominent along passive margins and the Bengal and Indus fans (Fig. DR1). A high sedimentation rate in the equatorial Pacific (Fig. DR1) is associated with rapid deposition of biogenic sediment underlying a zone of intense upwelling (Van Andel et al., 1975). A wide belt of rapid sedimentation rates (>5.5 cm/k.y.) along the Southeast Indian Ridge (SEIR) between 75°E and 150°E is a global anomaly (Fig. 1A; Fig. DR1). This region is far removed from the influence of high surface productivity (Soppa et al., 2014) and lithogenous input, experiences low to moderate vertical sediment flux (Fig. DR4), and occurs over young oceanic crust (Fig. DR3) adjacent to an abyssal plain where sedimentation rates would normally be close to the median global value. This belt is much more extensive than the area of sediment accumulation in the northern North Atlantic (Fig. DR1), which is linked to multiple contourite drifts (Rebesco et al., 2014). Overall, the short-term Holocene age model–derived sedimentation rates in the

Southern Ocean are moderately higher than the long-term rates (Fig. 1A; Fig. DR5), with a median difference of 1.7 cm/k.y. (Fig. DR5), and show a linear relationship with the focusing factors (Fig. 1C). This reflects a strong dependence of Southern Ocean Holocene sedimentation rates on lateral sediment redistribution. The focusing factors along the SEIR sedimentation rate anomaly are consistently >1 with a mean of 3 ± 2 (Fig. 2) and generally higher than elsewhere in the Southern Ocean (Fig. DR6).

DISCONFORMITIES

Five major fields of Holocene unconformities are evident in the Southern Ocean (Fig. 1B) (Dezileau et al., 2000; Kennett and Watkins, 1976; Ledbetter and Ciesielski, 1986; Osborn et al., 1983; Watkins and Kennett, 1972), with most occurring at latitudes higher than 50°S within regions where the sedimentation rate is very low (<1 cm/k.y.; Fig. DR7) and the water depth is 3–5 km (Figs. DR8 and DR9). The largest of these fields lies between 120°E and 165°E

and is associated with the SEIR and its triple junction with Macquarie and Pacific–Antarctic ridges (Fig. 1B). It occurs partly within the belt of anomalously high sedimentation rates (Fig. 1A; Fig. DR7) and within a region of mixed lithologies (Fig. DR10) characterized by relatively low CaCO₃ and high SiO₂ contents (Figs. DR11 and DR12). Smaller unconformity fields occur east of the Kerguelen Plateau and in the Weddell Sea, Bellingshausen, and Argentine basins (Fig. 1B) where the sedimentation rates are likewise low with nearby small pockets of anomalously high sedimentation rates (Fig. 1; Fig. DR7).

BOTTOM-WATER CURRENTS

The unconformity fields all overlap with areas of intense eddy activity where the bottom-current speeds and standard deviations exceed 0.1 m/s (Figs. 1B and 2) with a maximum of ~0.2 m/s. Bottom currents are steered by major bathymetric features (e.g., the Kerguelen Plateau, Fig. 2) due to Earth’s rotation, while smaller-scale

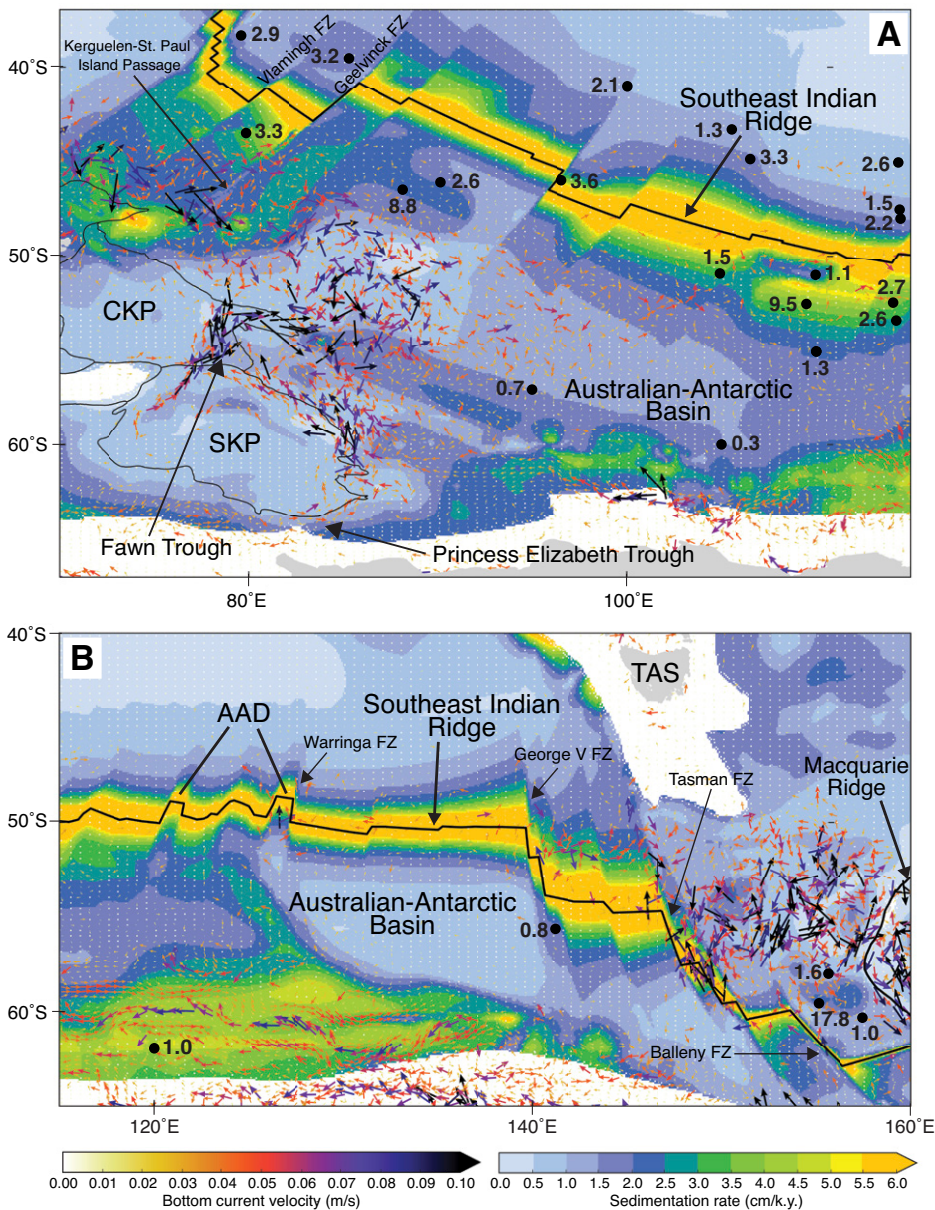


Figure 2. Quiver plot of modeled present-day bottom currents overlying long-term sedimentation rates and focusing factors (black circles) in the Southeast Indian Ridge region bounded by the Kerguelen Plateau to the west (A) and Macquarie Ridge to the east (B). Note that currents with very low velocities appear as white dots. CKP—Central Kerguelen Plateau; SKP—Southern Kerguelen Plateau; AAD—Australian-Antarctic Discordance; TAS—Tasmania; FZ—fracture zone. Equidistant cylindrical projection.

features (e.g., seamounts) may impinge or enhance current speeds (Rebesco et al., 2014). We focus on the SEIR because of a clear juxtaposition of extreme differences in sedimentation rates and the occurrence of distinct fields of sustained erosion linked to bottom-current activity (Dezileau et al., 2000; Kennett and Watkins, 1976; Osborn et al., 1983).

Our numerical model (Fig. 2) shows that the SEIR is bounded by two major regions of high bottom-current velocities whose occurrence coincides with areas of seafloor unconformities and low sedimentation rates ($\sim 1 \pm 0.5$ cm/k.y.; Fig. 2) and whose movement is confined by the

Kerguelen Plateau to the west (Fig. 2A) and by the Macquarie Ridge north of the Macquarie Triple Junction to the east (Fig. 2B; Figs. DR13 and DR14). The general flow direction through the Fawn Trough and the Kerguelen–St. Paul Island Passage (Fig. 2A) is northerly and easterly into the Australian-Antarctic Basin, consistent with schematic circulation patterns of McCartney and Donohue (2007). The eastern sector of the SEIR experiences severe seafloor erosion at the Warringa fracture zone boundary of the Antarctic-Australian Discordance and along the flanks of all major fracture zones between the George V and Balleny fracture zones (Fig.

2B). These regions are marked by high bottom-current velocities (~ 0.05 – 0.1 m/s) augmented by northerly flow due to the leakage of bottom currents from the southern to the northern side of the ridge (Fig. 2B) partly explaining the occurrence of patches of diatom ooze just north of these fracture zones (Fig. DR15).

The anomalously high rates of sediment accumulation along the SEIR are largely due to lateral transport of sediment from the two areas of high and variable bottom-current velocities (Figs. 1B and 2; Fig. DR16) favorable for generating intense nepheloid layers as much as 2 km thick (McCave, 1986) to regions where low bottom-current speeds (< 0.03 m/s; Fig. 2) allow fine particles to settle out of suspension (Rebesco et al., 2014; Stow et al., 2009). This is the case along most of the ~ 8000 -km-long segment of the SEIR between the Central Kerguelen Plateau and the Tasman fracture zone (Fig. 2), which underlies areas of low summer surface productivity with the exception of three short segments (Figs. DR17–DR20). Transport of sediment within this region is further supported by focusing factors $>> 1$ (Fig. 2; Table DR1).

We suggest that the anomalous accumulation of sediment along the SEIR represents a giant succession of contourite drifts that is a major extension of the much smaller contourite east of Kerguelen Plateau proposed by Dezileau et al. (2000). Bottom-current velocities in this region are consistent with velocities of $< \sim 0.06$ m/s expected for contourite drifts (Stow et al., 2009). Likewise, sedimentation rates (Figs. 1A and 1C; Table DR1) are within the low range of < 2 – 10 cm/k.y. expected for open-ocean pelagic contourite drifts (Stow et al., 2002). The distribution of regional unconformities at the base and within the drift (Fig. 1B) whose overall geometry is outlined by anomalously high sedimentation rates (Fig. 1A) is consistent with our numerical bottom-current model (Fig. 1B). This suggests that two SEIR regions (east of the Kerguelen Plateau and northwest of the Macquarie triple junction) have undergone long-term sustained erosion by locally persistent currents resulting in a gradual and extensive buildup of sediment along the entire ridge segment between them. This is supported by focusing factors ranging from 1.5 to 9 similar to previously mapped values northeast of Kerguelen Plateau (Dezileau et al., 2000). The age of the oldest crust subject to anomalous accumulation of sediment is ca. 3–5 Ma based on the oceanic crustal ages from Müller et al. (2016) and broadly consistent with the maximum ages of 2.5 Ma proposed by Kennett and Watkins (1976) and 4.4 Ma by Osborn et al. (1983) based on magnetostratigraphy.

CONCLUSIONS

Our combination of a high-resolution numerical ocean circulation model with geological observations from the seafloor allows us to

make a clear connection between two regions of extremely vigorous bottom currents (east of the Kerguelen Plateau and northwest of the Macquarie triple junction) and widespread disconformities. The intervening region along the SEIR reveals a major global sedimentation rate anomaly caused by excess sediment buildup in the absence of high surface productivity. This anomaly appears both in sedimentation rates derived from total sediment thickness that are consistent with Holocene age model-derived sedimentation rates as well as in focusing factors $>>1$ reflecting lateral redistribution of Holocene sediment. We suggest that an 8000-km-length of the SEIR crest overlying oceanic crust younger than 5 Ma is covered by a vast succession of hitherto unmapped Pliocene–Holocene contourite deposits. Ocean drilling of the inferred contourite drifts would provide a high-resolution record of Southern Ocean climate change.

ACKNOWLEDGMENTS

We are grateful to all shipboard scientists. We thank Tristan Salles and Nicky Wright for help with Python scripting. We thank Nicky Wright, three anonymous reviewers, and editor Judith Totman Parrish for their very constructive criticisms. This research was supported by the University of Sydney Faculty of Science Seed Grant (Dutkiewicz), the Australian Research Council (ARC) ITRP grant IH130200012 (Müller), and ARC Future FT120100842 (Hogg), and ARC DECRA DE150100223 (Spence) fellowships.

REFERENCES CITED

Carter, L., McCave, I.N., and Williams, M.J.M., 2009, Circulation and water masses of the Southern Ocean: A review, *in* Florindo, F., and Siebert, M., eds., *Developments in Earth and Environmental Sciences, Antarctic Climate Evolution, Volume 8*: Amsterdam, Elsevier, p. 85–114.

Chase, Z., and Burckle, L.H., 2015, Compilation of ^{230}Th -normalized opal burial and opal concentrations from Southern Ocean surface sediments: doi:10.1594/PANGAEA.846117.

Crosta, X., Romero, O., Armand, L.K., and Pichon, J.-J., 2005, The biogeography of major diatom taxa in Southern Ocean sediments: 2. Open ocean related species: *Palaeogeography, Palaeoclimatology, Palaeoecology*, v. 223, p. 66–92, doi:10.1016/j.palaeo.2005.03.028.

Dezileau, L., Bareille, G., Reyss, J.L., and Lemoine, F., 2000, Evidence for strong sediment redistribution by bottom currents along the southeast Indian ridge: *Deep-Sea Research, Part I: Oceanographic Research Papers*, v. 47, p. 1899–1936, doi:10.1016/S0967-0637(00)00008-X.

Francois, R., Frank, M., Rutgers van der Loeff, M.M., and Bacon, M.P., 2004, ^{230}Th normalization: An essential tool for interpreting sedimentary fluxes during the late Quaternary: *Paleoceanography*, v. 19, PA1018, doi:10.1029/2003PA000939.

Geibert, W., Rutgers van der Loeff, M.M., Usbeck, R., Gersonde, R., Kuhn, G., and Seeberg-Elverfeldt, J., 2005, Quantifying the opal belt in the Atlantic

and southeast Pacific sector of the Southern Ocean by means of ^{230}Th normalization: *Global Biogeochemical Cycles*, v. 19, GB4001, doi:10.1029/2005GB002465.

Goodell, H.G., and Watkins, N.D., 1968, The paleomagnetic stratigraphy of the Southern Ocean: 20° West to 160° East longitude: *Deep Sea Research and Oceanographic Abstracts*, v. 15, p. 89–112, doi:10.1016/0011-7471(68)90030-2.

Goodell, H.G., Houtz, R., Ewing, M., Hayes, D., Naini, B., Echols, R.J., Kennett, J.P., and Donahue, J., 1973, *Marine sediments of the southern oceans*: New York, American Geographical Society, *Antarctic Map Folio 17*, 9 plates.

Griffies, S.M., Biastoch, A., Böning, C., Bryan, F., Danabasoglu, G., Chassignet, E.P., England, M.H., Gerdes, R., Haak, H., and Hallberg, R.W., 2009, Coordinated ocean-ice reference experiments (COREs): *Ocean Modelling*, v. 26, p. 1–46, doi:10.1016/j.ocemod.2008.08.007.

Griffies, S.M., Winton, M., Anderson, W.G., Benson, R., Delworth, T.L., Dufour, C.O., Dunne, J.P., Goddard, P., Morrison, A.K., and Rosati, A., 2015, Impacts on ocean heat from transient mesoscale eddies in a hierarchy of climate models: *Journal of Climate*, v. 28, p. 952–977, doi:10.1175/JCLI-D-14-00353.1.

Huang, X., and Jokat, W., 2016, Middle Miocene to present sediment transport and deposits in the southeastern Weddell Sea, Antarctica: *Global and Planetary Change*, v. 139, p. 211–225, doi:10.1016/j.gloplacha.2016.03.002.

Kennett, J.P., and Watkins, N.D., 1976, Regional deep-sea dynamic processes recorded by late Cenozoic sediments of the southeastern Indian Ocean: *Geological Society of America Bulletin*, v. 87, p. 321–339, doi:10.1130/0016-7606(1976)87<321:RDDPRB>2.0.CO;2.

Kolla, V., Sullivan, L., Streeter, S.S., and Langseth, M.G., 1976, Spreading of Antarctic Bottom Water and its effects on the floor of the Indian Ocean inferred from bottom-water potential temperature, turbidity, and sea-floor photography: *Marine Geology*, v. 21, p. 171–189, doi:10.1016/0025-3227(76)90058-X.

Ledbetter, M.T., and Ciesielski, P.F., 1986, Post-Miocene disconformities and paleoceanography in the Atlantic sector of the Southern Ocean: *Palaeogeography, Palaeoclimatology, Palaeoecology*, v. 52, p. 185–214, doi:10.1016/0031-0182(86)90046-5.

McCartney, M.S., and Donohue, K.A., 2007, A deep cyclonic gyre in the Australian–Antarctic Basin: *Progress in Oceanography*, v. 75, p. 675–750, doi:10.1016/j.pocean.2007.02.008.

McCave, I.N., 1986, Local and global aspects of the bottom nepheloid layers in the world ocean: *Netherlands Journal of Sea Research*, v. 20, p. 167–181, doi:10.1016/0077-7579(86)90040-2.

Meredith, M.P., Woodworth, P.L., Chereskin, T.K., Marshall, D.P., Allison, L.C., Bigg, G.R., Donohue, K., Heywood, K.J., Hughes, C.W., and Hibbert, A., 2011, Sustained monitoring of the Southern Ocean at Drake Passage: Past achievements and future priorities: *Reviews of Geophysics*, v. 49, RG4005, doi:10.1029/2010RG000348.

Müller, R.D., et al., 2016, Ocean basin evolution and global-scale plate reorganization events

since Pangea breakup: *Annual Review of Earth and Planetary Sciences*, v. 44, p. 107–138, doi:10.1146/annurev-earth-060115-012211.

Osborn, N.I., Ciesielski, P.F., and Ledbetter, M.T., 1983, Disconformities and paleoceanography in the southeast Indian Ocean during the past 5.4 million years: *Geological Society of America Bulletin*, v. 94, p. 1345–1358, doi:10.1130/0016-7606(1983)94<1345:DAPITS>2.0.CO;2.

Rebesco, M., Hernández-Molina, F.J., Van Rooij, D., and Wählin, A., 2014, Contourites and associated sediments controlled by deep-water circulation processes: State-of-the-art and future considerations: *Marine Geology*, v. 352, p. 111–154, doi:10.1016/j.margeo.2014.03.011.

Soppa, M.A., Hirata, T., Silva, B., Dinter, T., Peeken, I., Wiegmann, S., and Bracher, A., 2014, Global retrieval of diatom abundance based on phytoplankton pigments and satellite data: *Remote Sensing*, v. 6, p. 10,089–10,106, doi:10.3390/rs61010089.

Stow, D.A.V., Faugères, J.-C., Howe, J.A., Pudsey, C.J., and Viana, A.R., 2002, Bottom currents, contourites and deep-sea sediment drifts: Current state-of-the-art, *in* Stow, D.A.V., et al., eds., *Deep-Water Contourite Systems: Modern Drifts and Ancient Series, Seismic and Sedimentary Characteristics*: Geological Society of London Memoir 22, p. 7–20, doi:10.1144/GSL.MEM.2002.022.01.02.

Stow, D.A.V., Hernández-Molina, F.J., Llave, E., Sayago-Gil, M., del Río, V.D., and Branson, A., 2009, Bedform-velocity matrix: The estimation of bottom current velocity from bedform observations: *Geology*, v. 37, p. 327–330, doi:10.1130/G25259A.1.

Van Andel, T.H., Heath, G.R., and Moore, T.C., 1975, Cenozoic History and Paleoceanography of the Central Equatorial Pacific Ocean: A Regional Synthesis of Deep Sea Drilling Project Data: *Geological Society of America Memoir 143*, 223 p., doi:10.1130/MEM143-p1.

Watkins, N.D., and Kennett, J.P., 1972, Regional sedimentary disconformities and Upper Cenozoic changes in bottom water velocities between Australasia and Antarctica, *in* Hayes, D.E., ed., *Antarctica Oceanology II: The Australian–New Zealand Sector*: American Geophysical Union Antarctic Research 19, p. 273–293, doi:10.1029/AR019p0273.

Watkins, N.D., and Kennett, J.P., 1977, Erosion of deep-sea sediments in the Southern Ocean between longitudes 70°E and 190°E and contrasts in manganese nodule development: *Marine Geology*, v. 23, p. 103–111, doi:10.1016/0025-3227(77)90084-6.

Whittaker, J.M., Goncharov, A., Williams, S.E., Müller, R.D., and Leitchenkov, G., 2013, Global sediment thickness data set updated for the Australian–Antarctic Southern Ocean: *Geochemistry Geophysics Geosystems*, v. 14, p. 3297–3305, doi:10.1002/ggge.20181.

Manuscript received 25 May 2016

Revised manuscript received 8 June 2016

Manuscript accepted 15 June 2016

Printed in USA

Appendix DR1. Description of sedimentological datasets, Table DR1, Figures DR1-DR20

Vigorous deep-sea currents cause global anomaly in sediment accumulation in the Southern Ocean

Adriana Dutkiewicz*, R. Dietmar Müller, Andrew McC. Hogg, and Paul Spence

*corresponding author: adriana.dutkiewicz@sydney.edu.au

DATASETS

Holocene sediment ages

Our unconformity-conformity dataset was supplemented by dated sediment cores from the Southern Ocean not found in the Chase and Burckle (2015) dataset. The sediment cores are: PS2090-1 and PS1654-2 (Bianchi and Gersonde, 2004a; Bianchi and Gersonde, 2004b; Bianchi and Gersonde, 2004c), MD07-3076 (Skinner et al., 2010a, b), RC11-83 (Charles and Fairbanks, 1992a; Charles and Fairbanks, 1992b), MD84-551, MD84-527 and MD73-025 (Labracherie et al., 1989a, b; Labracherie et al., 1989c), MD88-770 (Labeyrie et al., 1996a, b), MR0806-PC09, MD07-3128 and 202-1233 (Lamy et al., 2015a, b, c, d), PS2038-2, PS1821-6 and PS1575-1 (Bonn et al., 1998a, b, c, d), OSO0910_KC04, OSO0910_KC09, OSO0910_KC10, OSO0910_KC15, OSO0910_KC19, OSO0910_KC23 and DF81_PC07 (Kirshner et al., 2012a, b), RC12-225 and MD84-529 (Howard and Prell, 1994a, b; Howard and Prell, 1994c), GOMEA-06, GOMEA-14, GOMEA-15 and GOMEA-16 (Gozhik et al., 1991a, b), PS2082 and PS1506-1 (Mackensen et al., 1994a, b, c), PS75/083-1, PS75/079-2, PS75/076-2, PS75/074-3, PS75/059-2 and PS75/056-1 (Lamy et al., 2014a, b, c, d, e, f, g), TSP-2MC, TSP-3MC and TSP-2PC (Murayama et al., 2000a, b), TTN057-13-PC4 (Shemesh et al., 2002a, b), RC13-229, MD88-769 and MD80-304 (Rosenthal et al., 1995a, b, c, d), KC073 (Allen et al., 2005a, b), DF79.012-GB, DF79.009-GB, Core302 and 119-740A (Domack et al., 1991a, b, c, d, e), MD03-2597, NBP01-01-KC17B and NBP01-01-JPC17B (Maddison et al., 2012a, b), PS1380-3 (Grobe and Mackensen, 1992a, b), PS1786-1, PS2606-6 and PS58/271-1 (Jacot Des Combes et al., 2008a, b).

We carefully reviewed all *Eltanin* sites from Watkins and Kennett (1972) that had been re-analyzed by Osborn et al. (1983) and in rare instances of discrepancies in polarity assignment we use the Osborn et al. (1983) ages as the polarity measurements were made using a more sensitive magnetometer and with improved biostratigraphic control. There is very good agreement between the Bruhnes-age assignment of the majority of *Eltanin* core tops dated by magnetostratigraphy and by subsequent more highly-resolved methods (Chase and Burckle, 2015). Rare exceptions include *Eltanin* cores E14-5 and E20-10 which were very well-dated by Chase et al. (2003) and contradicted the earlier results of Goodell and Watkins (1968); in these cases the Chase et al. (2003) dates are used.

Focusing factors

Focusing factors were calculated using the simplified equation from Dezileau et al. (2000):

$$\psi = \frac{F}{F_{vertical}}$$

where $F_{vertical}$ is the sediment rain rate ($\text{g}/\text{cm}^2/\text{ka}$) for an age-dated stratigraphic section; F is the accumulation rate ($\text{g}/\text{cm}^2/\text{ka}$); ψ is the focusing factor (Dezileau et al., 2000; Francois et al., 1993; Francois et al., 2004; Suman and Bacon, 1989). The accumulation rates were calculated from linear sedimentation segments from wells in which the age model is derived from ^{14}C dating, oxygen isotopes or a combination of oxygen isotopes and biostratigraphy and/or ^{14}C dating (see Table DR1 for list of cores) and dry bulk density for a given sample. Dry bulk densities were calculated using known CaCO_3 content and the best-fit second-order polynomial relationship of Froelich et al. (1991):

$$B_D = (5.313 \times 10^{-5}) \times (\text{CaCO}_3)^2 + (9.346 \times 10^{-4}) \times (\text{CaCO}_3) + 0.3367$$

where B_D is dry bulk density (g/cm^3). In the absence of CaCO_3 measurements for a small number of cores (see Table DR1), a mean dry bulk density of 0.4 g cm^{-3} for siliceous sediment (Geibert et al., 2005) was used. All values of $F_{vertical}$ (i.e., ^{230}Th -normalized sediment flux) were obtained from references cited in Table DR1. As most of the cores contain multiple measurements of CaCO_3 and corresponding ^{230}Th -normalized sediment flux over the interval of interest, our focusing factors are averages over those intervals.

Errors for focusing factors are very difficult to estimate and are rarely reported. For example, values given in Dezileau et al. (2000) and Frank et al. (1999) are given without errors although Frank et al. (1999) suggests that ψ is meaningful if it is significantly smaller (i.e., $< 50\%$) or greater (i.e., $> 50\%$) than 1. For core MD88-773, Yu (1994) gives an error range of ± 0.3 for focusing factors of 9.5 and 3.2. Despite uncertainties, Francois et al. (2004) argue that focusing factors are good proxies for sediment focusing.

Table DR1. Location, water depth, sedimentation rates and focusing factors (average over the interval of interest) for cores from the Southern Ocean. Sedimentation rates and focusing factors are for the Holocene (defined as 0-13 ka by Delzileau et al. (2003) and applied here for comparability reasons) except in the case of Yu (1994) data where the values represent the period 0-18 ka. Values in bold are from cited references, all other values were calculated using age models and ^{230}Th -normalized mass fluxes from cited references. *CaCO₃ measurement not available. See supplementary text for detail.

Core	Lat.	Long.	Water Depth (m)	Sedimentation rate (cm/kyr)	Focusing factor	Reference
E11-3	-56.90	-115.24	4023	2	2.5	Bradtmitter et al. (2009)
E11-4*	-57.83	-115.22	4774	1.4	1.3	Bradtmitter et al. (2009)
E11-7*	-60.92	-114.78	5029	2	1.2	Bradtmitter et al. (2009)
E11-12*	-65.87	-115.08	4718	1	0.7	Bradtmitter et al. (2009)
E14-16	-58.99	-125.03	4499	10	5.8	Bradtmitter et al. (2009)
E14-17	-57.83	-124.95	3904	6.5	5.3	Bradtmitter et al. (2009)
E15-4	-59.02	-99.76	4910	5	5.8	Bradtmitter et al. (2009)
E15-5	-58.02	-99.98	4307	2.5	3.7	Bradtmitter et al. (2009)
E15-6	-59.97	-101.32	4517	2	1.8	Bradtmitter et al. (2009)
E15-12	-58.68	-108.80	4572	1	0.6	Bradtmitter et al. (2009)
E15-28	-56.02	-149.82	3328	2	1	Bradtmitter et al. (2009)
E17-7	-61.08	-134.35	4435	2	0.7	Bradtmitter et al. (2009)
E19-6*	-61.93	-107.96	5064	1	0.6	Bradtmitter et al. (2009)
E19-7	-62.16	-109.09	5051	2.5	1	Bradtmitter et al. (2009)
E20-13	-55.00	-104.95	3895	1	1.6	Bradtmitter et al. (2009)
E21-20*	-60.25	-120.17	4701	3.3	1.6	Bradtmitter et al. (2009)
E23-14	-63.82	-108.85	4957	1	0.5	Bradtmitter et al. (2009)
E23-17*	-60.22	-114.63	5026	2	0.9	Bradtmitter et al. (2009)
E23-18	-58.98	-115.00	5272	2	0.9	Bradtmitter et al. (2009)
E25-16	-56.15	-156.22	3621	2.5	1.5	Bradtmitter et al. (2009)
E27-23	-59.62	155.24	3182	43.5	17.8	Bradtmitter et al. (2009)
E33-19	-59.86	-119.66	4389	2.5	1.2	Bradtmitter et al. (2009)
E36-36	-60.39	157.53	2816	3.8	1	Bradtmitter et al. (2009)
RC8-71	-58.05	155.73	3224	2.6	1.6	Bradtmitter et al. (2009)
VM16-115	-55.68	141.28	3147	2.4	0.8	Bradtmitter et al. (2009)
VM16-121	-50.67	164.38	3614	5.1	1.5	Bradtmitter et al. (2009)
VM17-88*	-57.03	-74.48	4063	1.3	0.2	Bradtmitter et al. (2009)
VM17-90*	-60.13	-74.93	4568	0.6	0.4	Bradtmitter et al. (2009)
VM18-73*	-61.53	-73.28	4568	1.8	1.4	Bradtmitter et al. (2009)
VM18-93	-59.48	-64.78	3834	1.6	0.9	Bradtmitter et al. (2009)
MD 94-102	-43.50	79.80	3205	5.9	3.3	Dezileau et al. (2000)
MD 94-104	-46.50	88.10	3460	12.5	8.8	Dezileau et al. (2000)
MD 88-769	-46.10	90.10	3420	4.1	2.6	Dezileau et al. (2000)
MD 88-770	-46.00	96.50	3290	6.8	3.6	Dezileau et al. (2000)
MD 84-527	-43.50	51.20	3269	27	10	Dezileau et al. (2000); Francois et al. (1993)
MD 88-773	-52.55	109.50	2460	27.4	9.5	Yu (1994)
MD 84-552	-54.90	73.80	1780	22.1	5	Dezileau et al. (2000)
PS1772-8	-55.46	1.16	4137	1.3	0.6	Frank et al. (1999); Frank (2002b)

Core	Lat.	Long.	Water Depth (m)	Sedimentation rate (cm/kyr)	Focusing factor	Data Reference
PS1768-8	-52.59	4.48	3299	13.75	4.6	Frank et al. (1999); Mackensen (1996)
PS1756-5	-48.90	6.71	3828	7.5	0.7	Frank et al. (1999); Frank and Mackensen (2002a)
PS1754-1	-46.77	7.61	2519	1.7	1.2	Frank et al. (1999); Frank (2002a)
PS2082-1	-43.22	11.74	4610	2.6	2	Frank et al. (1999); Frank and Mackensen (2002b)
PS2498-1	-44.15	-14.23	3783	6.3	5.7	Frank et al. (1999); Mackensen et al. (2001a)
PS2499-5	-46.51	-15.33	3175	2.9	2.2	Frank et al. (1999); Mackensen et al. (2001b)
E49-29	-57.10	94.96	4237	2.4	0.7	Yu (1994) and references therein
E48-3	-41.02	100.01	3930	1.4	2.1	Yu (1994) and references therein
E50-8	-50.93	104.91	3227	9.4	1.5	Yu (1994) and references therein
E45-27	-43.31	105.55	3776	1.6	1.3	Yu (1994) and references therein
E45-29	-44.88	106.52	3863	2.6	3.3	Yu (1994) and references therein
E49-6	-51.01	109.99	3326	2.3	1.1	Yu (1994) and references therein
E49-8	-55.07	110.02	3693	5.9	1.3	Yu (1994) and references therein
E45-64	-52.48	114.09	3823	8.1	2.7	Yu (1994) and references therein
E45-63	-53.44	114.26	3915	8.2	2.6	Yu (1994) and references therein
E45-79	-45.06	114.37	4079	1.9	2.6	Yu (1994) and references therein
E45-74	-47.55	114.44	3744	1.4	1.5	Yu (1994) and references therein
E45-71	-48.03	114.49	3658	2.1	2.2	Yu (1994) and references therein
E49-8	-55.07	110.02	3693	5.9	1.3	Yu (1994) and references therein
E48-13	-28.31	93.30	3380	5.9	8.8	Yu (1994) and references therein
E48-11	-29.40	97.32	3462	1.7	1.0	Yu (1994) and references therein
E48-27	-38.33	79.54	3285	2.9	2.9	Yu (1994) and references therein
E48-22	-39.54	85.25	3378	3.7	3.2	Yu (1994) and references therein
E50-13	-60.00	105.00	4209	2.1	0.3	Yu (1994) and references therein
E50-17	-62.00	120.03	4081	5.1	1.0	Yu (1994) and references therein

CaCO₃ and bSiO₂ content of surface sediments

Our maps of CaCO₃ and bSiO₂ percentages in surface sediments are based on combined datasets from Chase and Burckle (2015), Archer (1996), Archer (1999) and Bohrmann (1999).

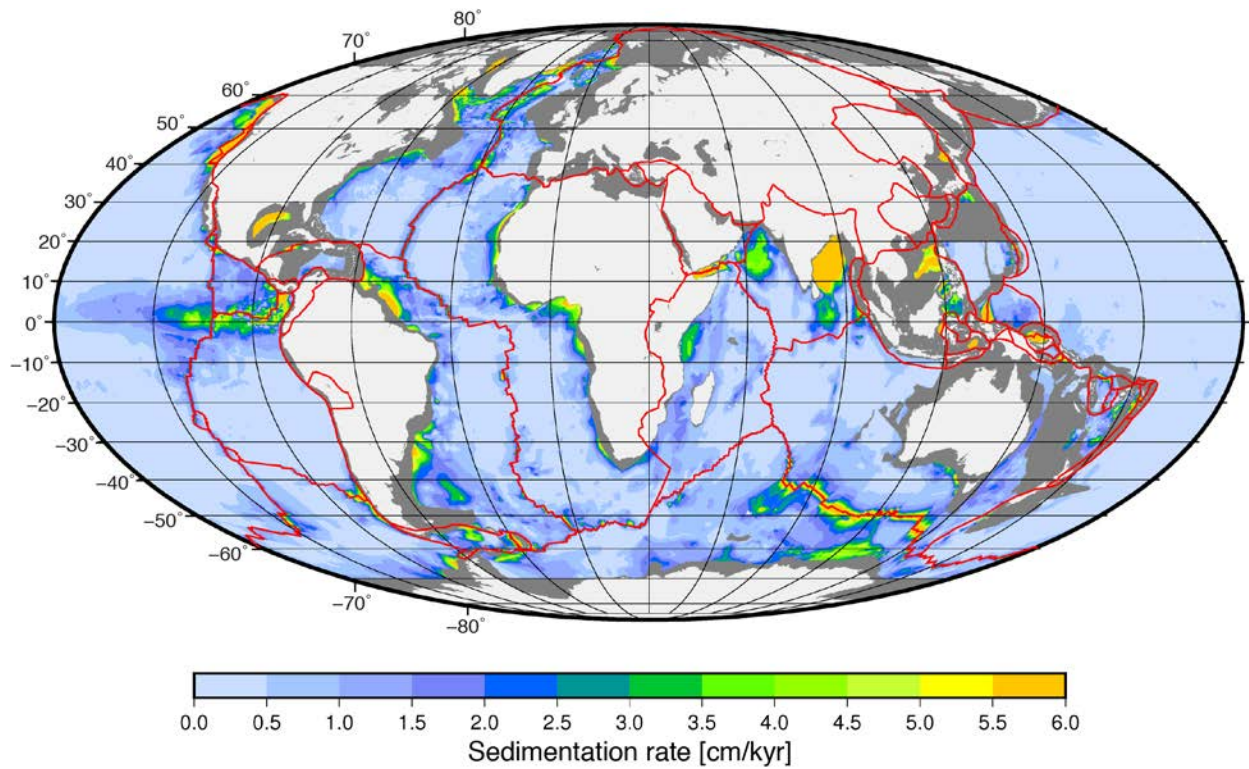


Figure DR1. Long-term average sedimentation rates in the world's ocean calculated using the global sediment thickness dataset of Whittaker et al. (2013) incorporating the dataset of Divins (2004), which represent minimum sediment thickness estimates, and the age grid of Müller et al. (2016). Red lines indicate plate boundaries. See also Figs. DR2 and DR3. Mollweide projection.

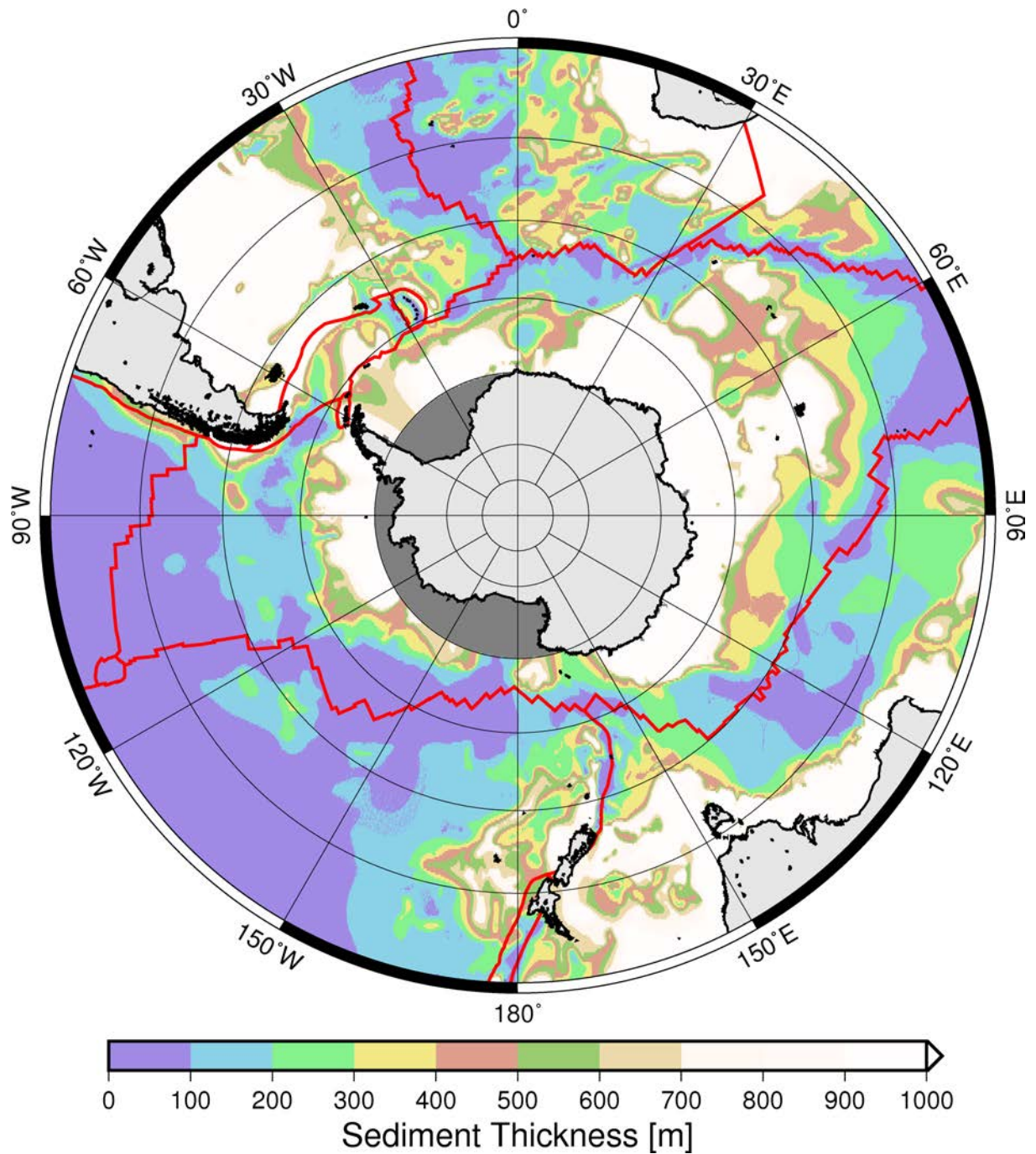


Figure DR2. Minimum sediment thickness estimates based on the global sediment thickness dataset of Whittaker et al. (2013) incorporating the dataset of Divins (2004). Red lines indicate plate boundaries. Stereographic projection.

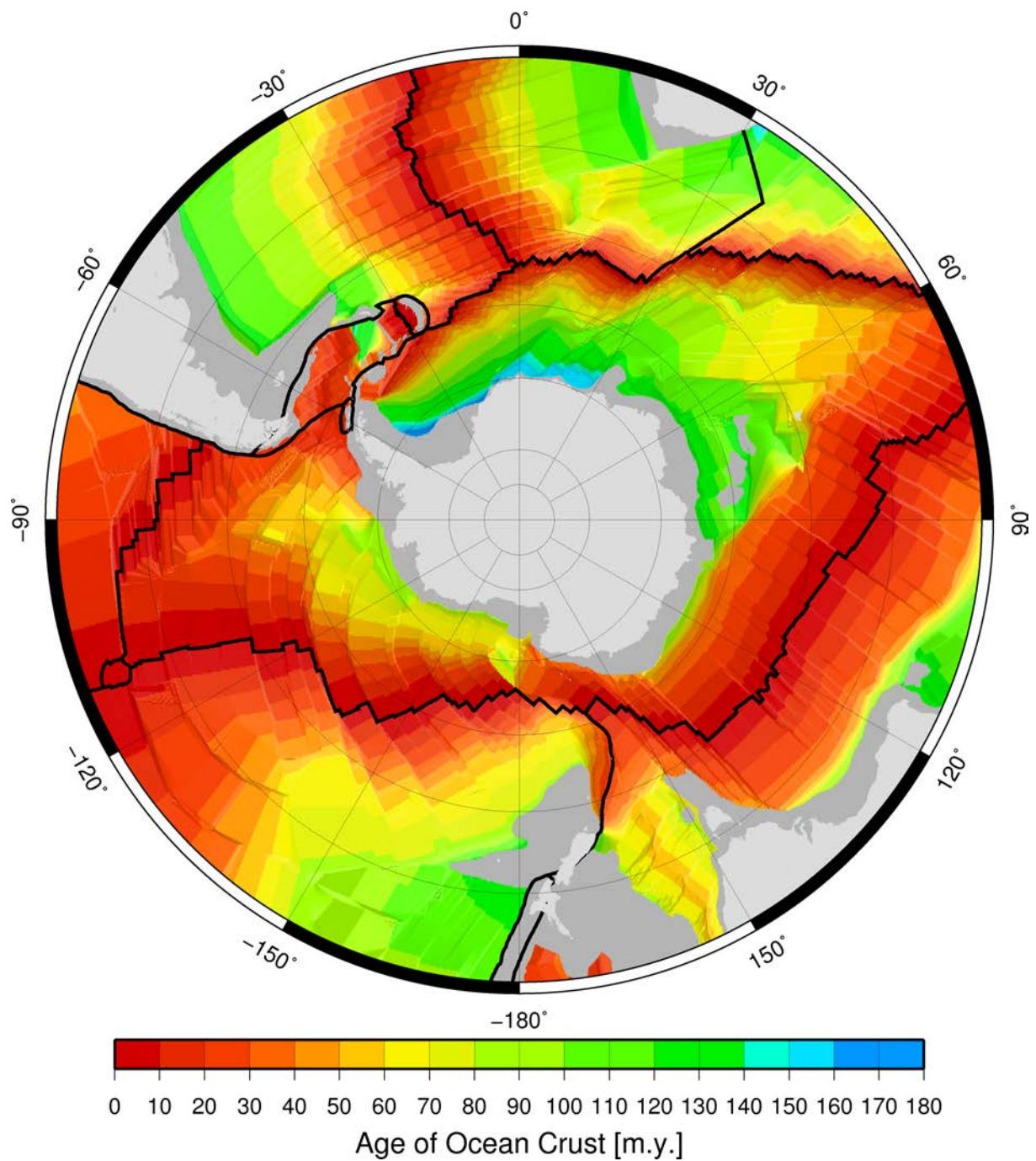


Figure DR3. Age of ocean crust from Müller et al. (2016). Black lines indicate plate boundaries with subaerial portions of continents shown in light grey and submerged continental crust in medium grey. Stereographic projection.

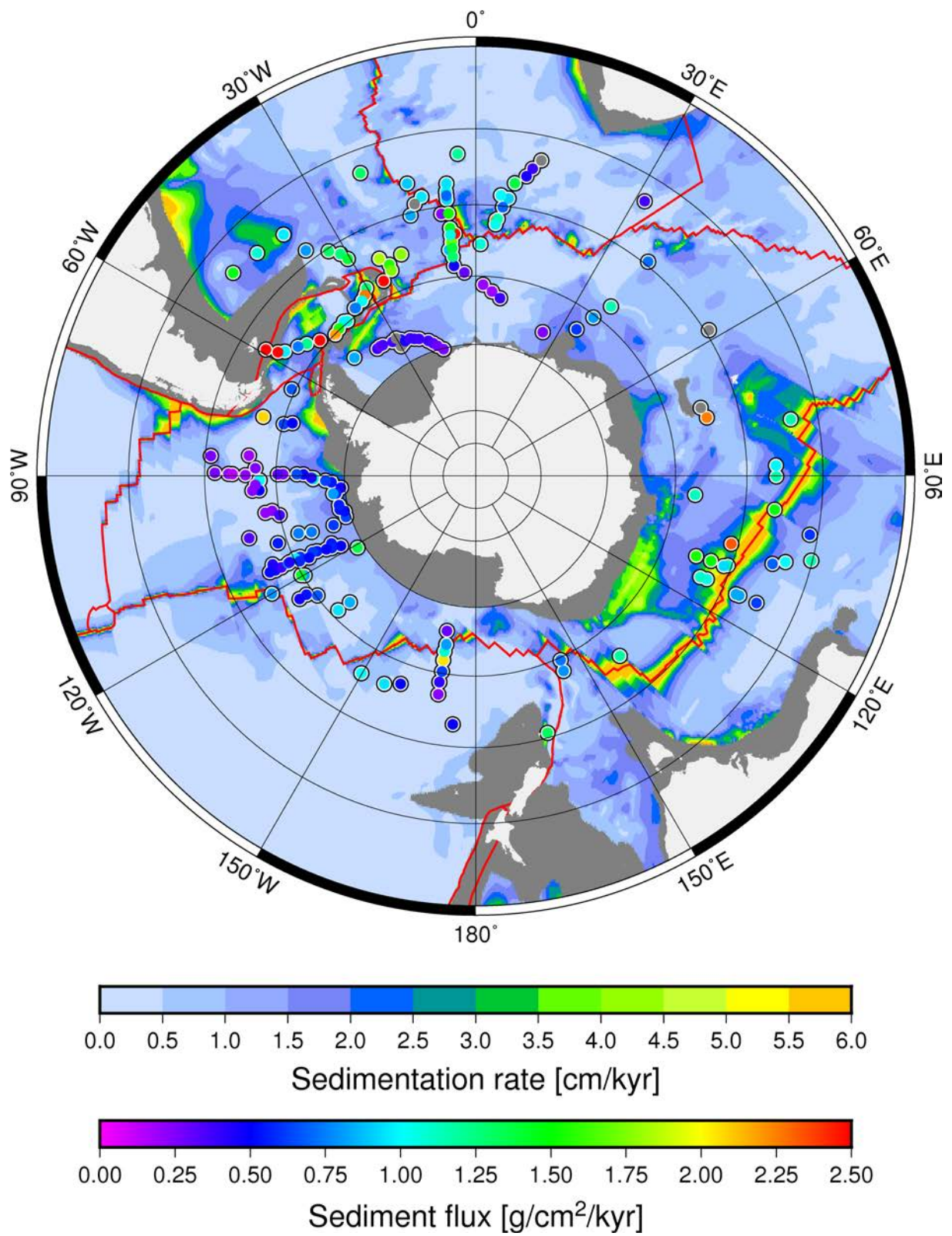


Figure DR4. Th-normalized sediment flux (circles) from Chase and Burckle, (2015) over long-term average sedimentation rates as in Figure DR1. Red lines indicate plate boundaries. Stereographic projection.

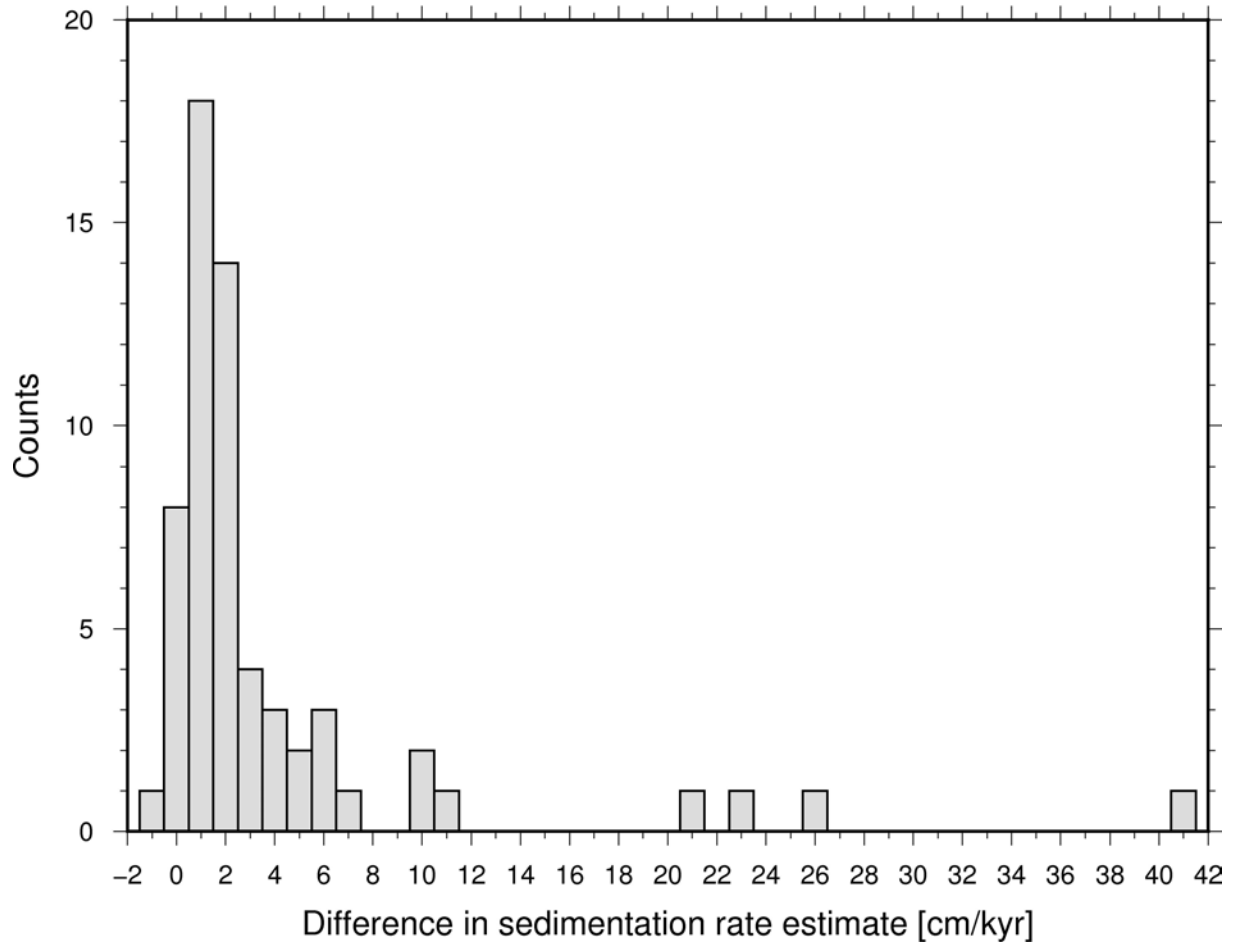


Figure DR5. Difference in sedimentation rate calculated using long-term average sedimentation rate (see Fig. DR1 caption for detail) minus Holocene sedimentation rate calculated using age-models for cores listed in Table DR1. The median difference is 1.7 cm/kyr, with a mean difference of 4 cm/kyr reflecting the influence of outliers due to high Holocene sedimentation rates at some locations (see Fig. 1A).

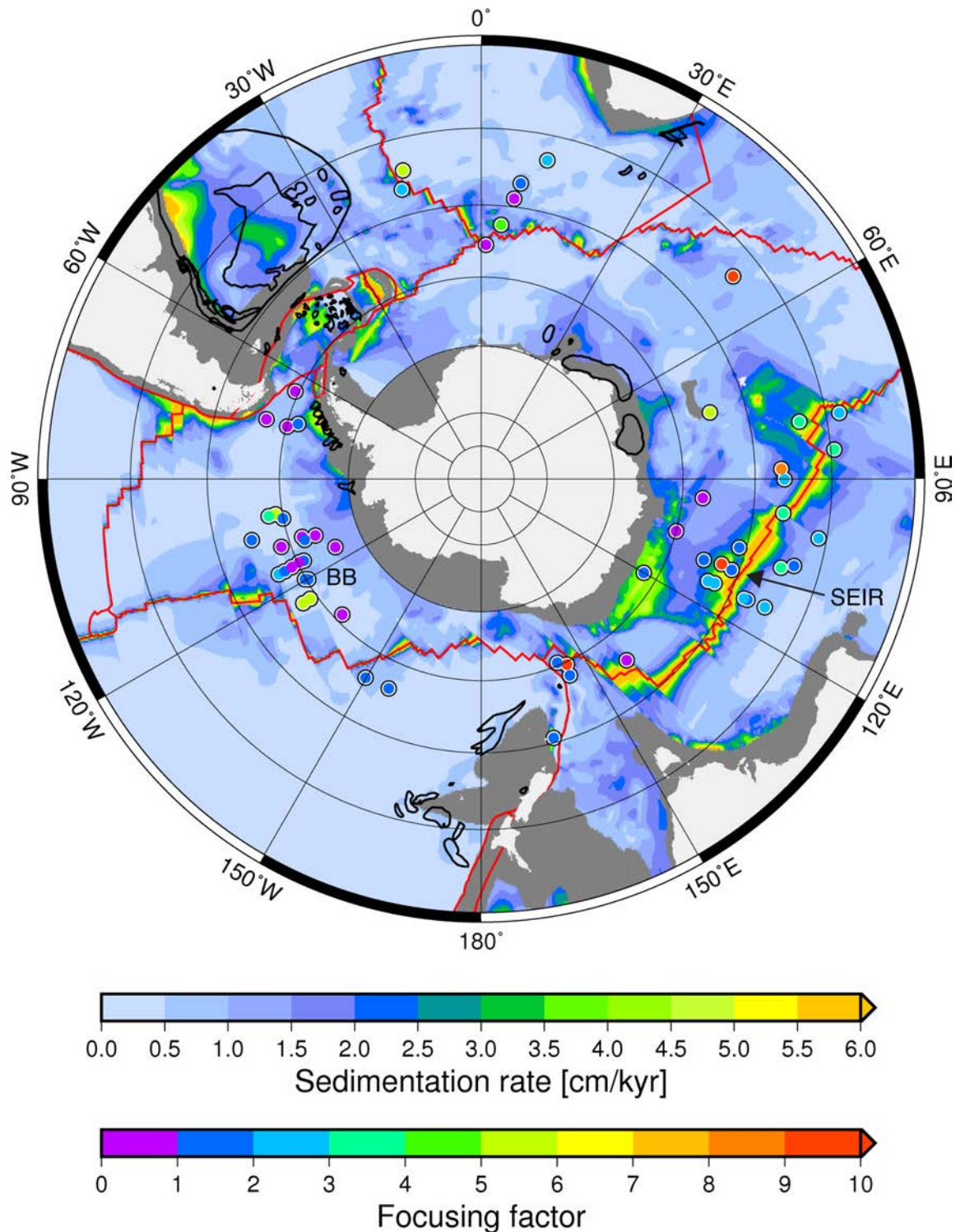


Figure DR6. Focusing factors (colored circles) overlying long-term sedimentation rates in the Southern Ocean. Focusing factors along the Southeast Indian Ridge (SEIR) are consistently and significantly greater than 1. In the Bellingshausen Basin (BB) the majority of focusing factors range between 0.5 and 1.5 with only 3 values > 5. Data in other parts of the Southern Ocean are relatively sparse. Black outlines indicate known large contourite deposits from Rebesco et al. (2014) available at <http://www.marineregions.org/>. Red lines denote plate boundaries. Stereographic projection.

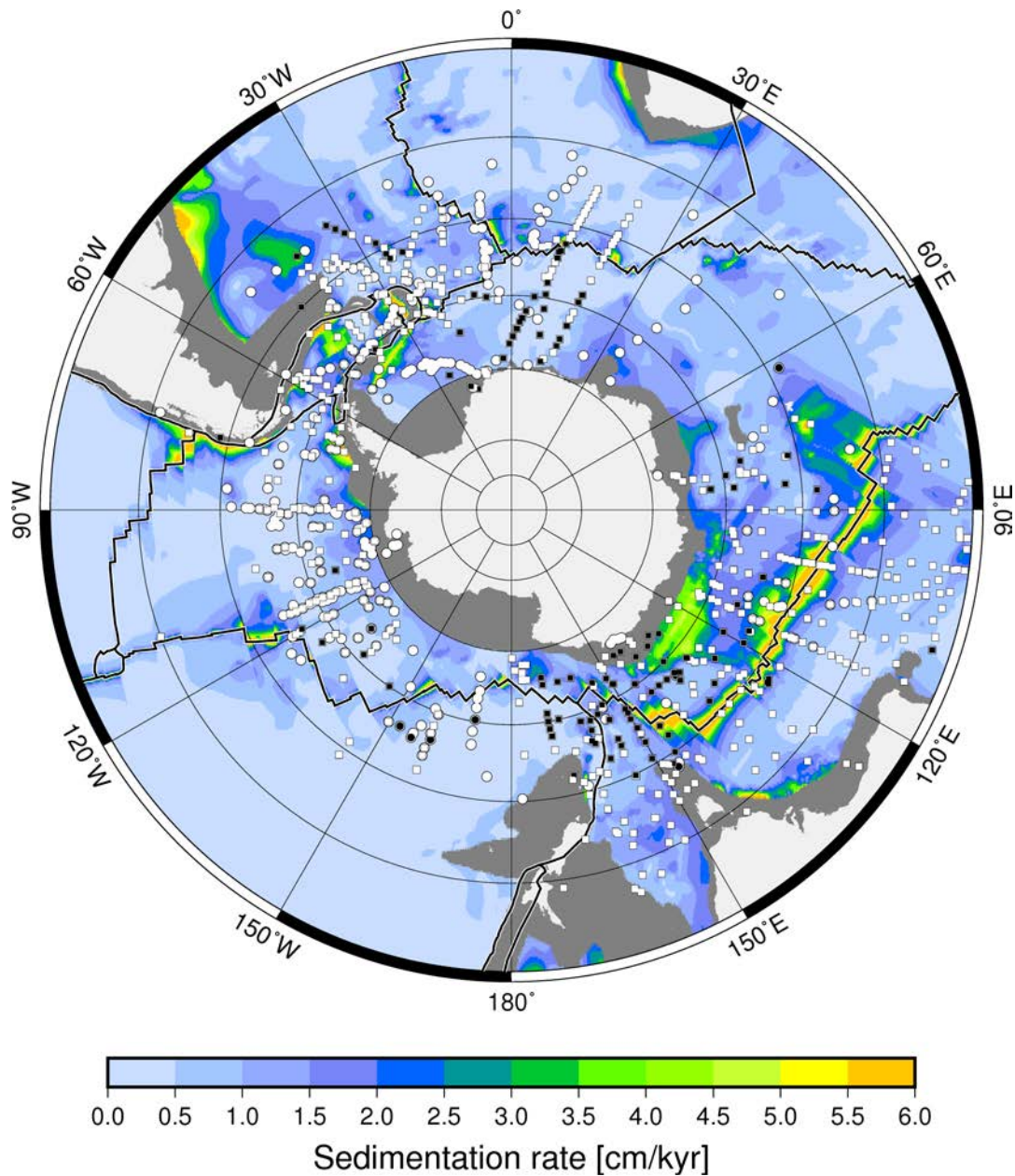


Figure DR7. Long-term average sedimentation rates overlain by conformities (white squares and white circles) and unconformities (black squares and black circles) in surface sediment of Bruhnes age. Squares represent magnetostratigraphic data from Watkins and Kennett (1972), Kennett and Watkins (1976), Osborn et al. (1983) and Ledbetter and Ciesielski (1986). Circles represent Holocene sediment dated by ^{14}C and undisturbed surface sediment from the Chase et al. (2015) compilation as well as additional data from various sources (see section on datasets in this Data Repository). Black lines denote plate boundaries. Stereographic projection.

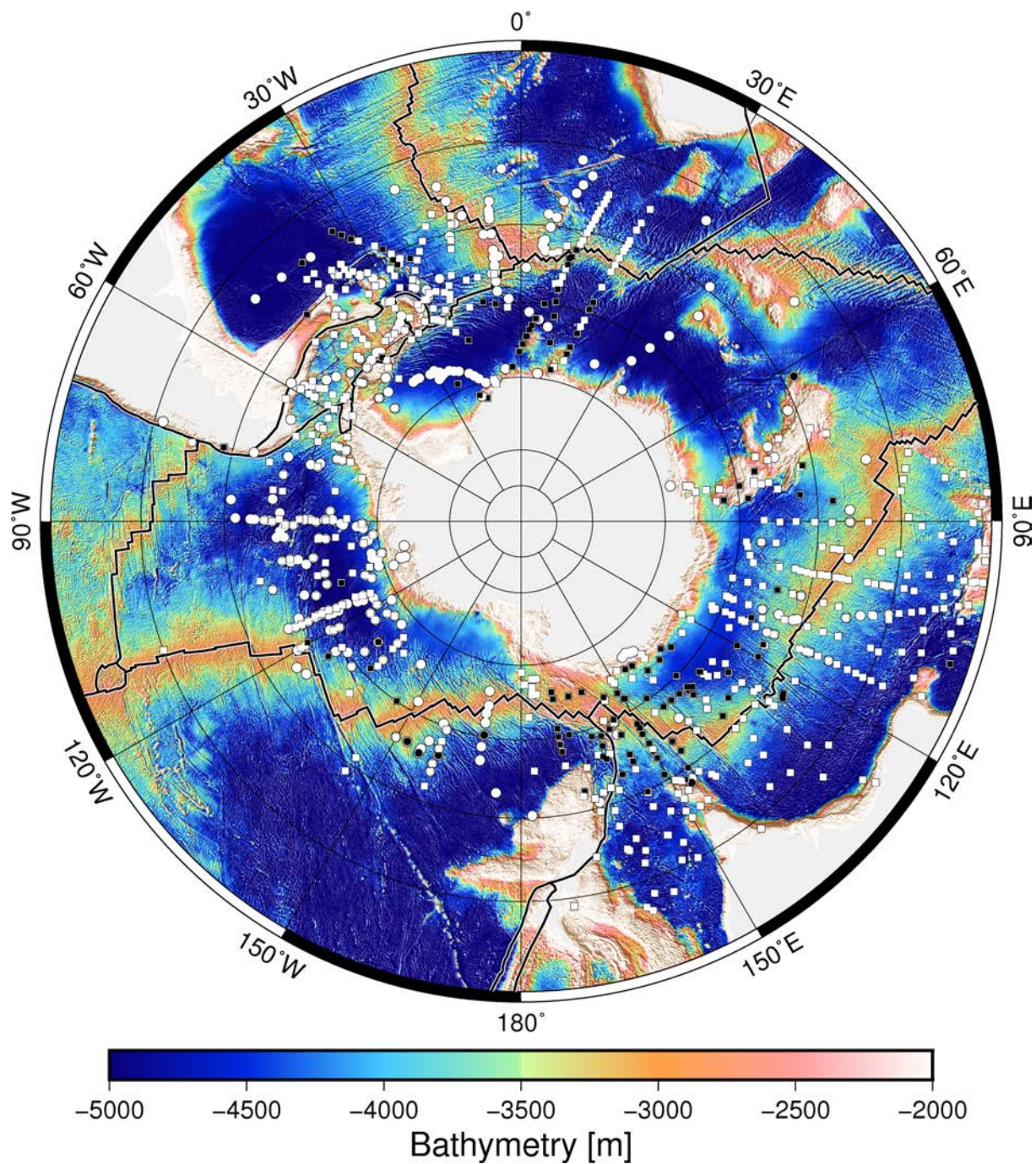


Figure DR8. Bathymetry overlain by conformities (white squares and white circles) and unconformities (black squares and black circles) in surface sediment of Brunhes age. See caption in Fig. DR7 for detail. Black lines with white outlines denote plate boundaries. Bathymetry is from the ETOPO1 E 1 Arc-Minute Global Relief Model (Amante and Eakins, 2009). Stereographic projection.

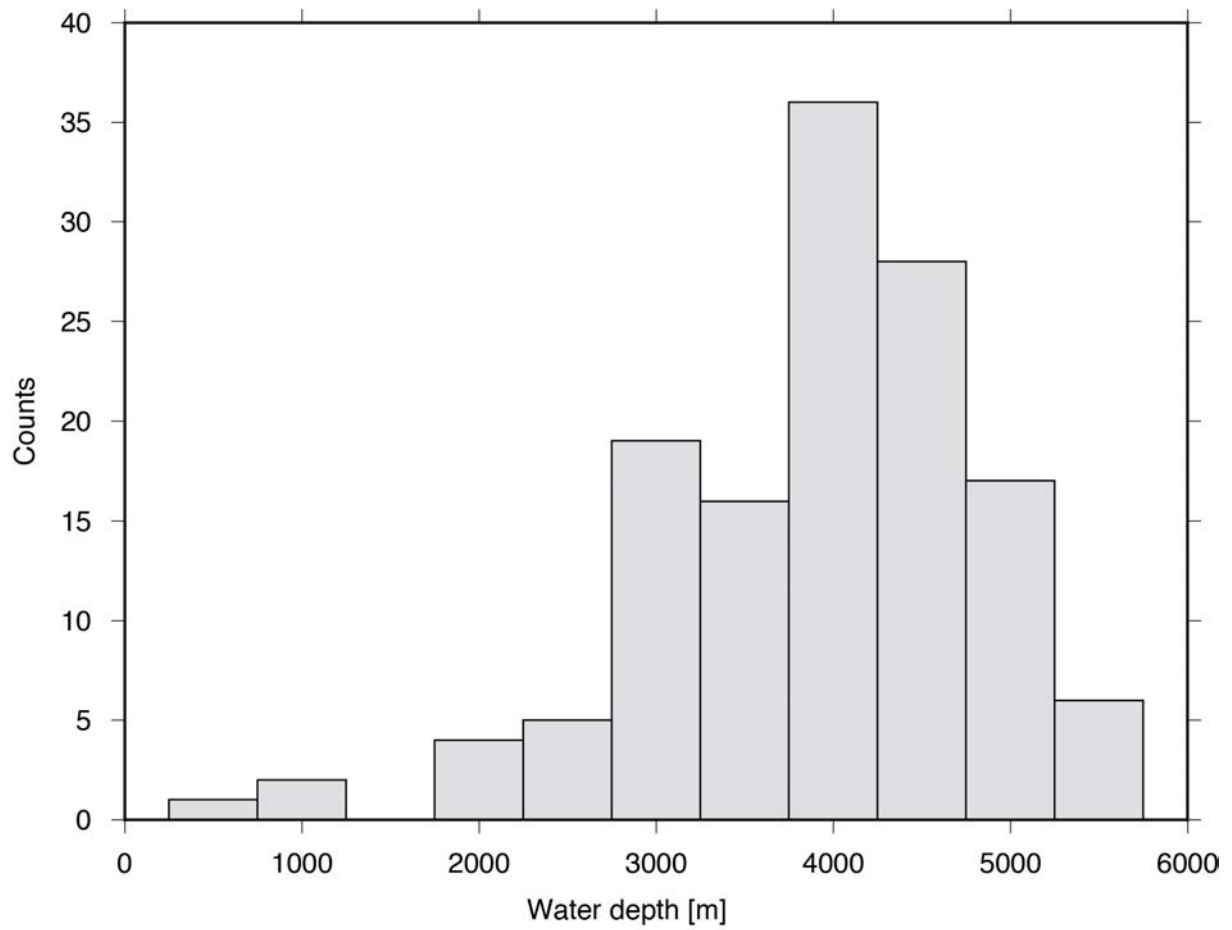


Figure DR9. Frequency of Brunhes age unconformity occurrence versus depth for the Southern Ocean. See caption for Figure DR7 for detail.

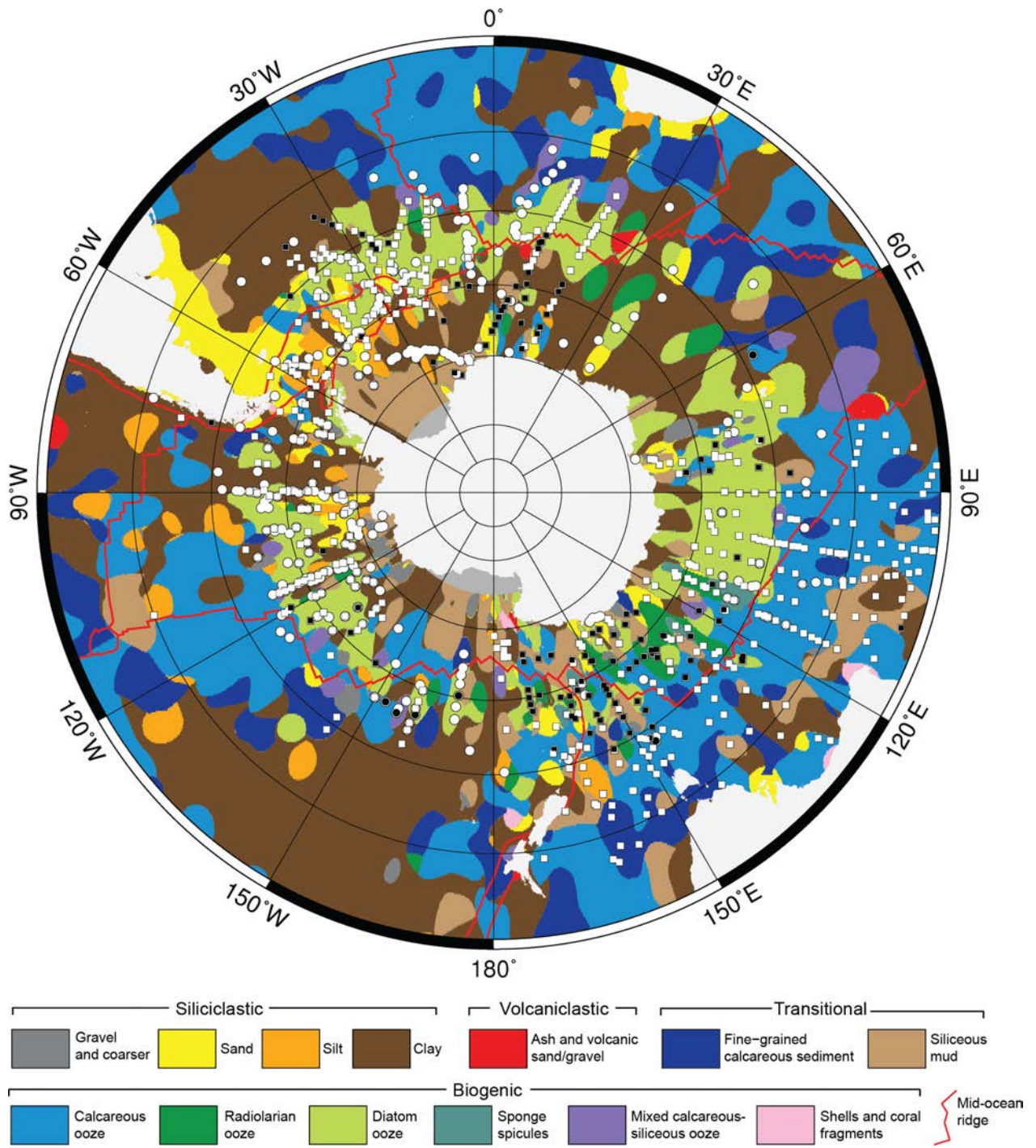


Figure DR10. Seafloor lithologies from Dutkiewicz et al. (2015) overlay by conformities (white squares and white circles) and unconformities (black squares and black circles) in surface sediment of Bruhnes age (see Fig. DR7 caption for detail). Stereographic projection.

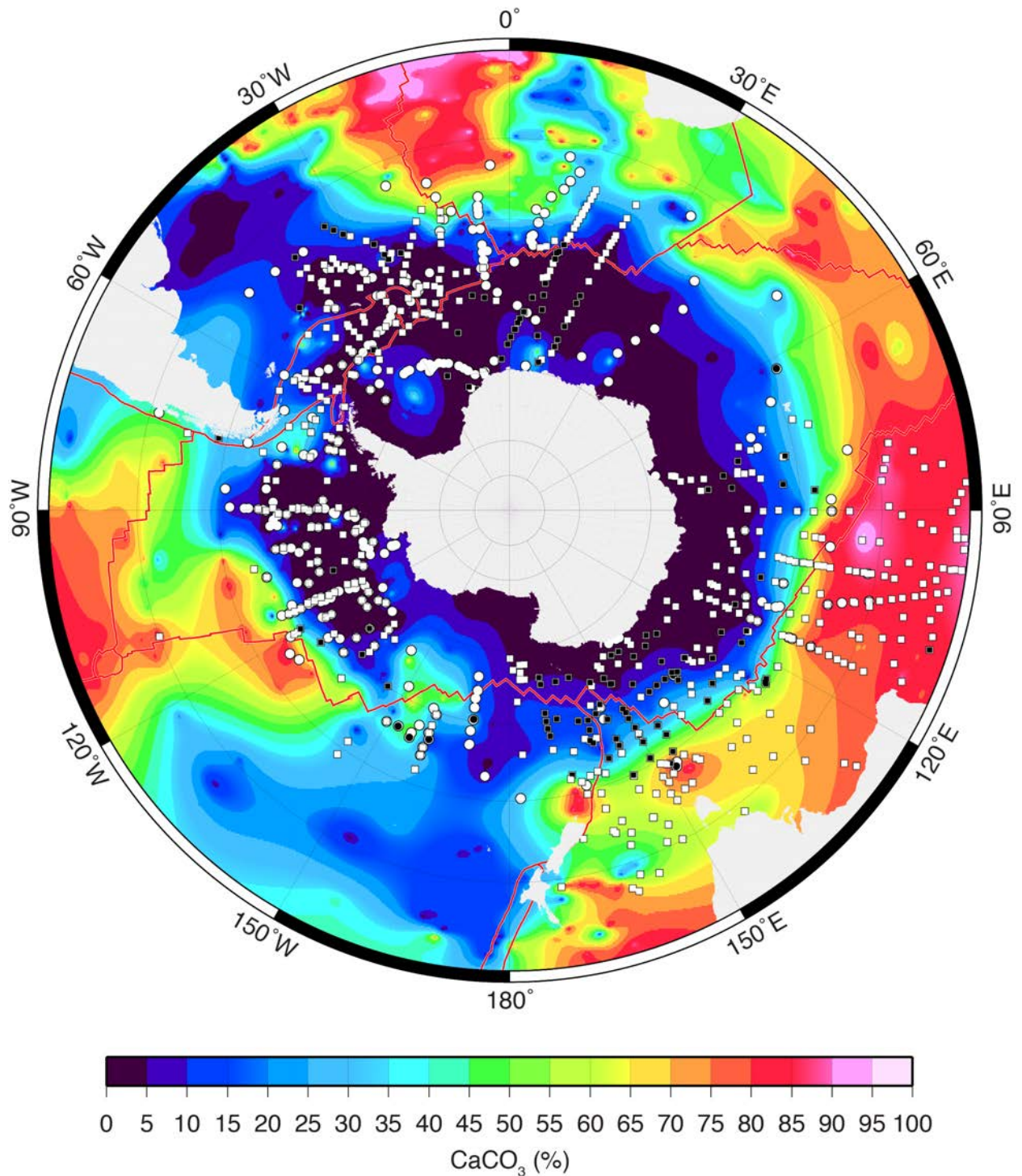


Figure DR11. Gridded map of CaCO₃ concentrations in surface sediments using combined data from Archer (1999), Bohrmann (1999) and Chase and Burckle (2015) overlain by conformities (white squares and white circles) and unconformities (black squares and black circles) in surface sediment of Brunhes age (see Fig. DR7 caption for detail). Red lines denote plate boundaries. Gridding was done using an anisotropic spline with tension of 0.5. Stereographic projection.

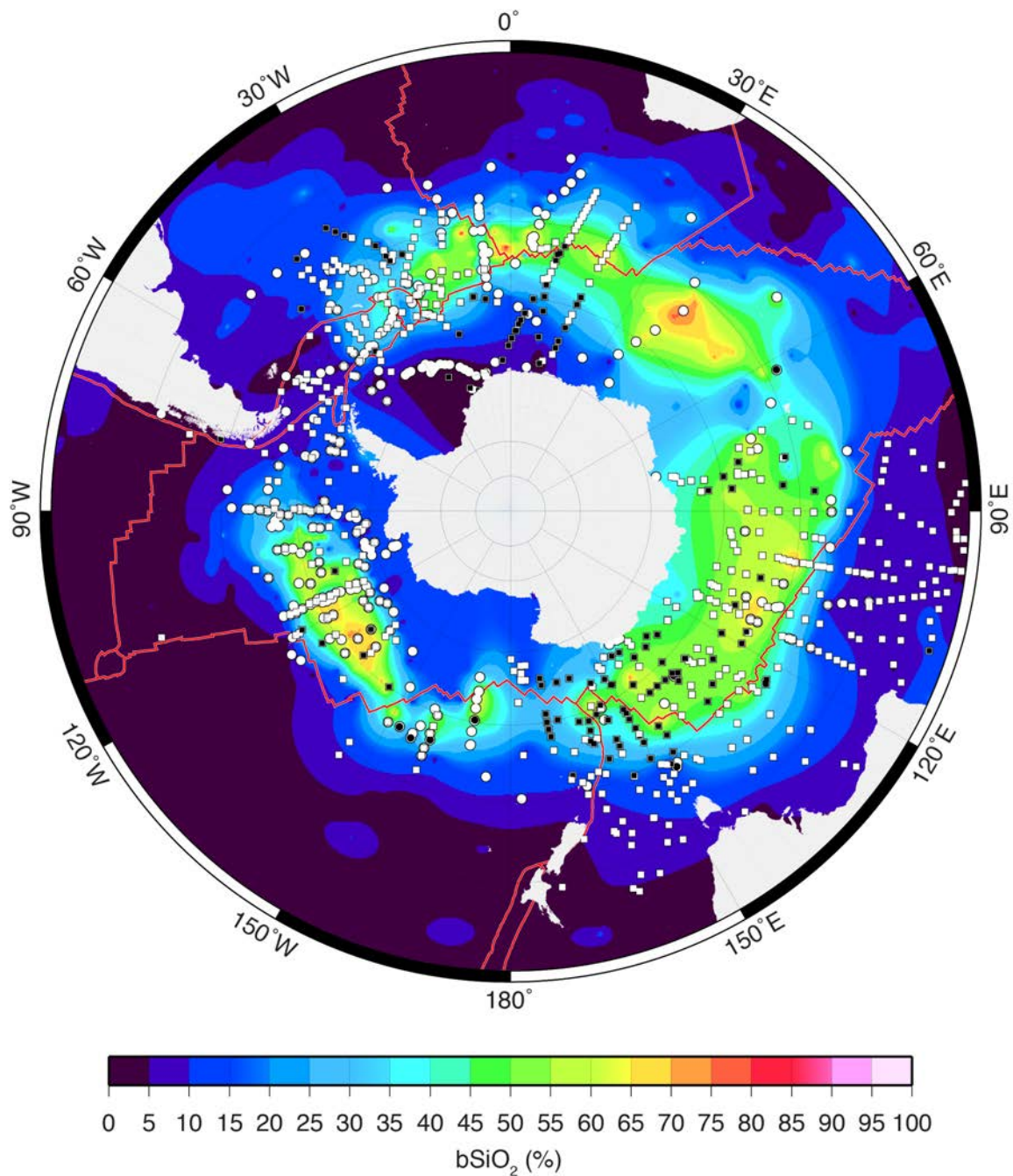


Figure DR12. Gridded map of bSiO₂ concentrations in surface sediments using combined data from Archer (1999), Bohrmann (1999) and Chase and Burckle (2015) overlain by conformities (white squares and white circles) and unconformities (black squares and black circles) in surface sediment of Bruhnes age (see Fig. DR7 caption for detail). Red lines denote plate boundaries. Gridding was done using an anisotropic spline with tension of 0.5. Stereographic projection.

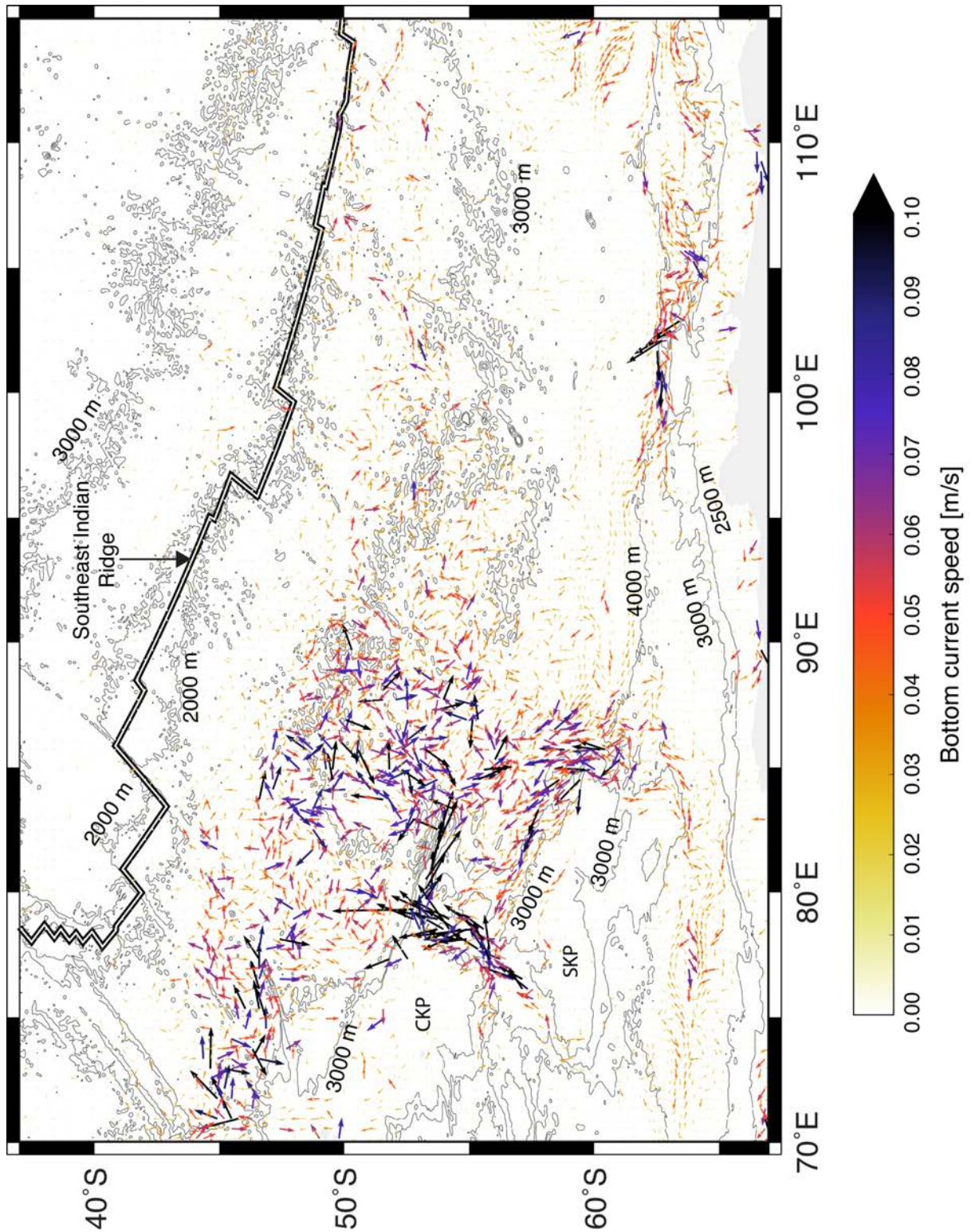


Figure DR13. Quiver plot overlying bathymetry contours for the western sector of the Southeast Indian Ridge. CKP – Central Kerguelen Plateau, SKP – Southern Kerguelen Plateau. Equidistant cylindrical projection.

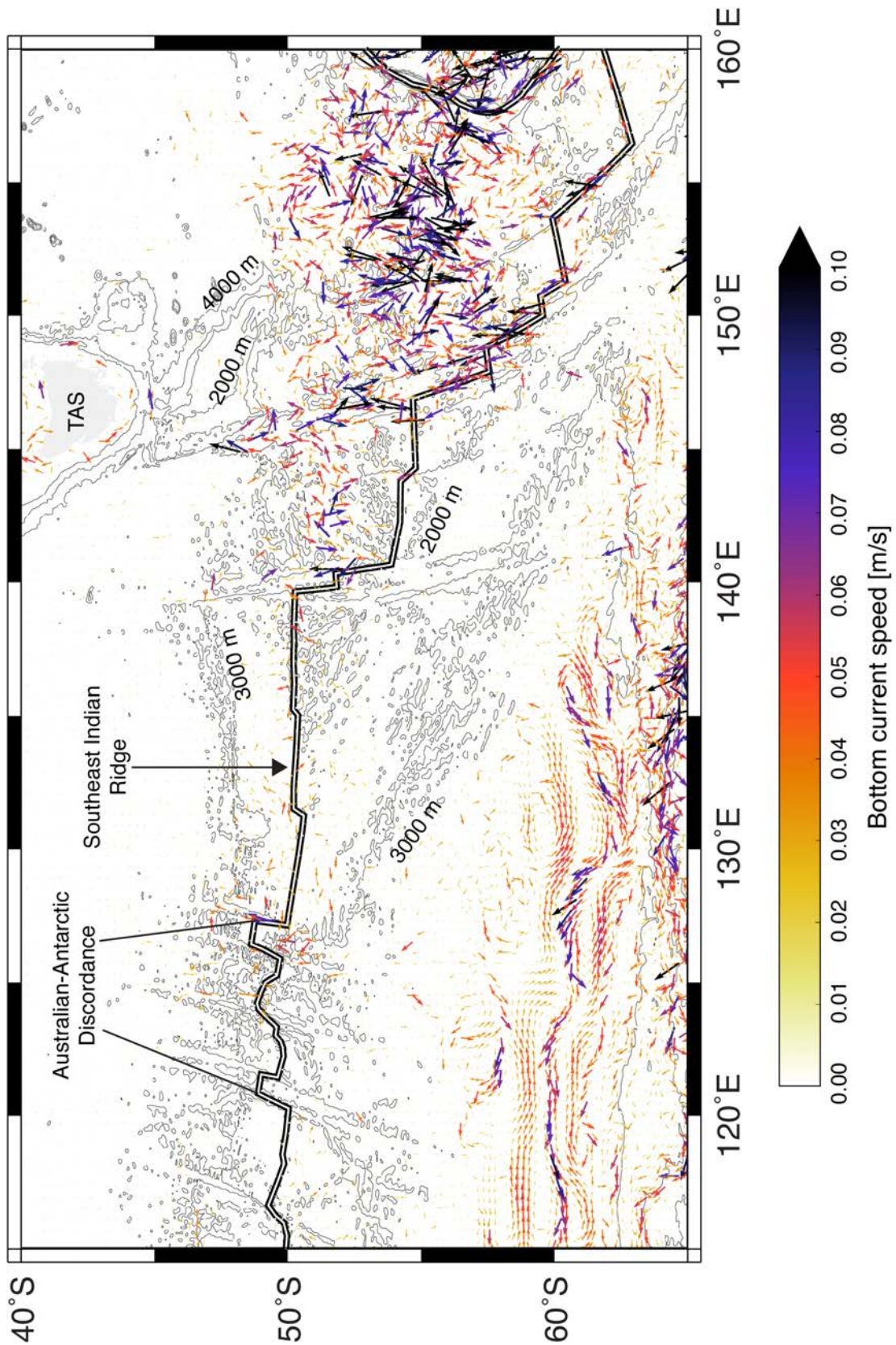


Figure DR14. Quiver plot overlying bathymetry contours for the eastern sector of the Southeast Indian Ridge. Equidistant cylindrical projection.

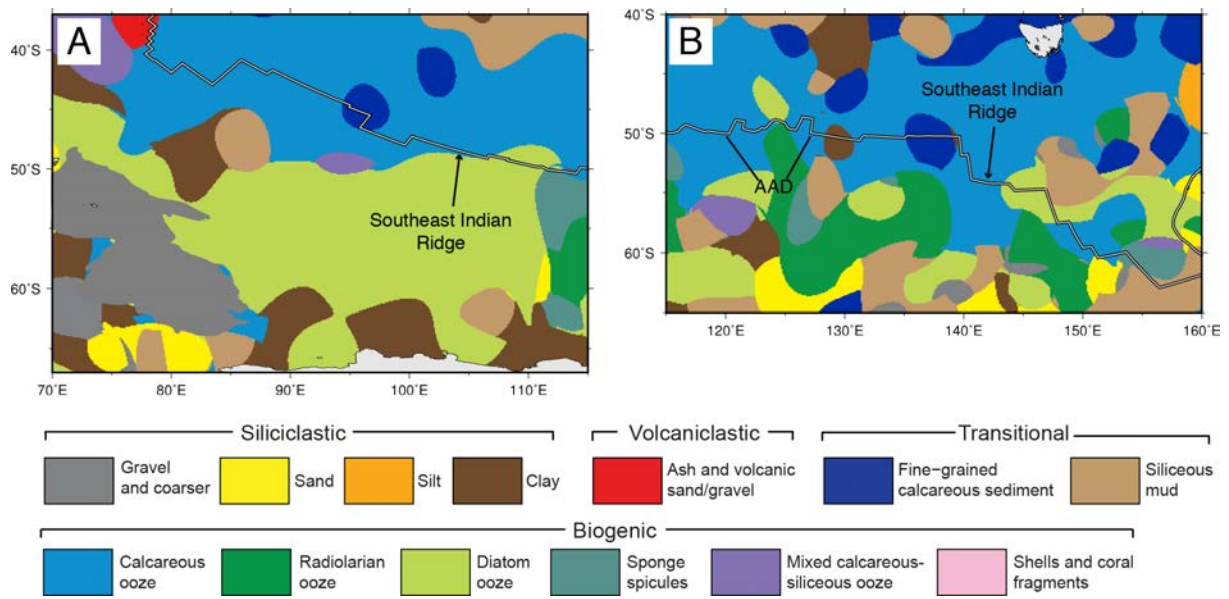


Figure DR15. Seafloor lithology from Dutkiewicz (2015) for the Southeast Indian Ridge region of the Southern Ocean. Equidistant cylindrical projection.

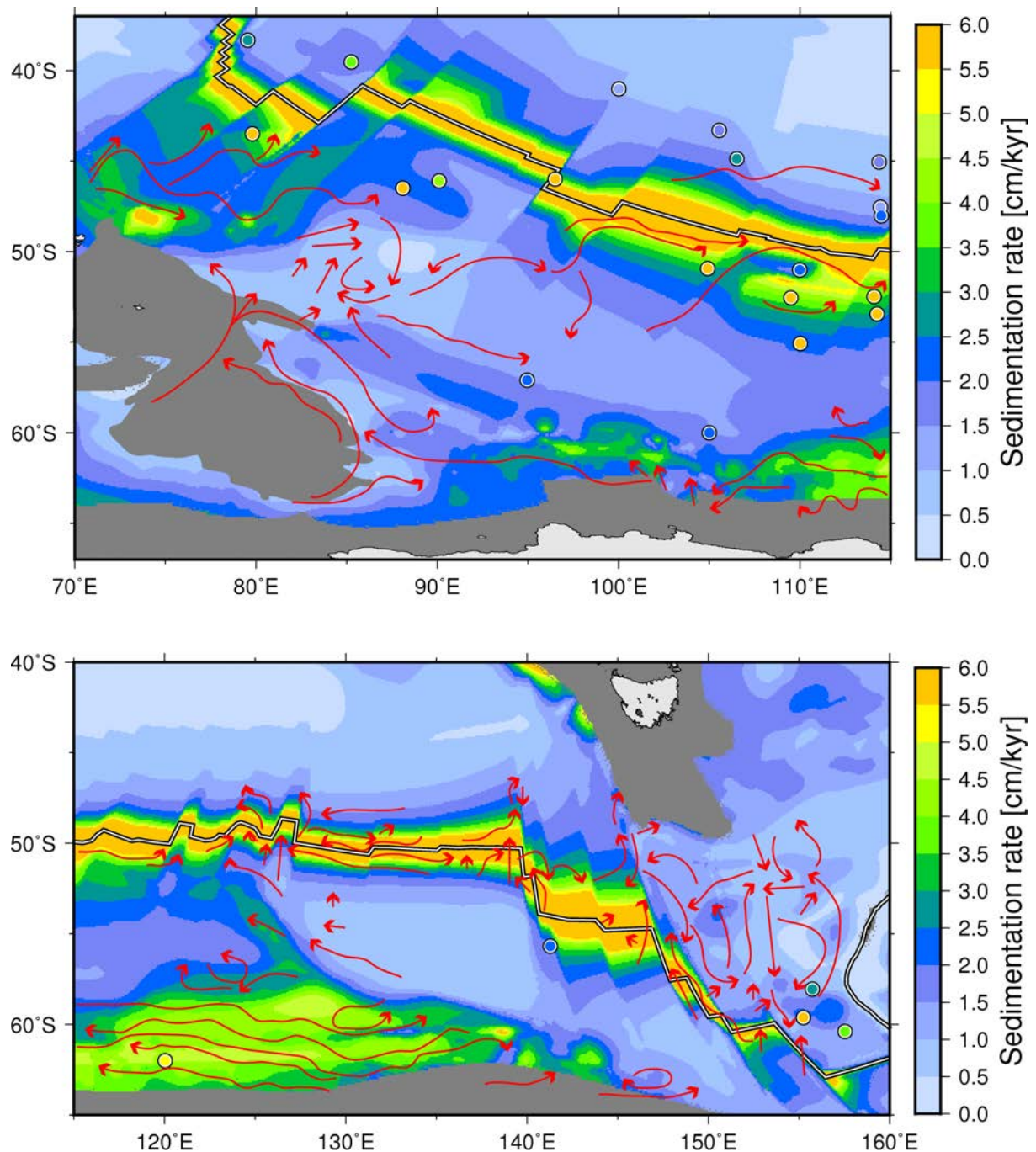


Figure DR16. Long-term average sedimentation rates in the Southern Ocean overlain with Holocene age-model derived sedimentation rates. Excess deposition of recent sediments along a mid-ocean ridge is expressed as bands of anomalously high sedimentation rates when computed by dividing the total sediment thickness by crustal age, with rates decreasing away from the mid-ocean ridge crest as the age of the crust increases. Black-white lines indicate plate boundaries. Red arrows indicate generalized bottom current directions based on quiver plots in Figs DR13 and 14. Equidistant cylindrical projection.

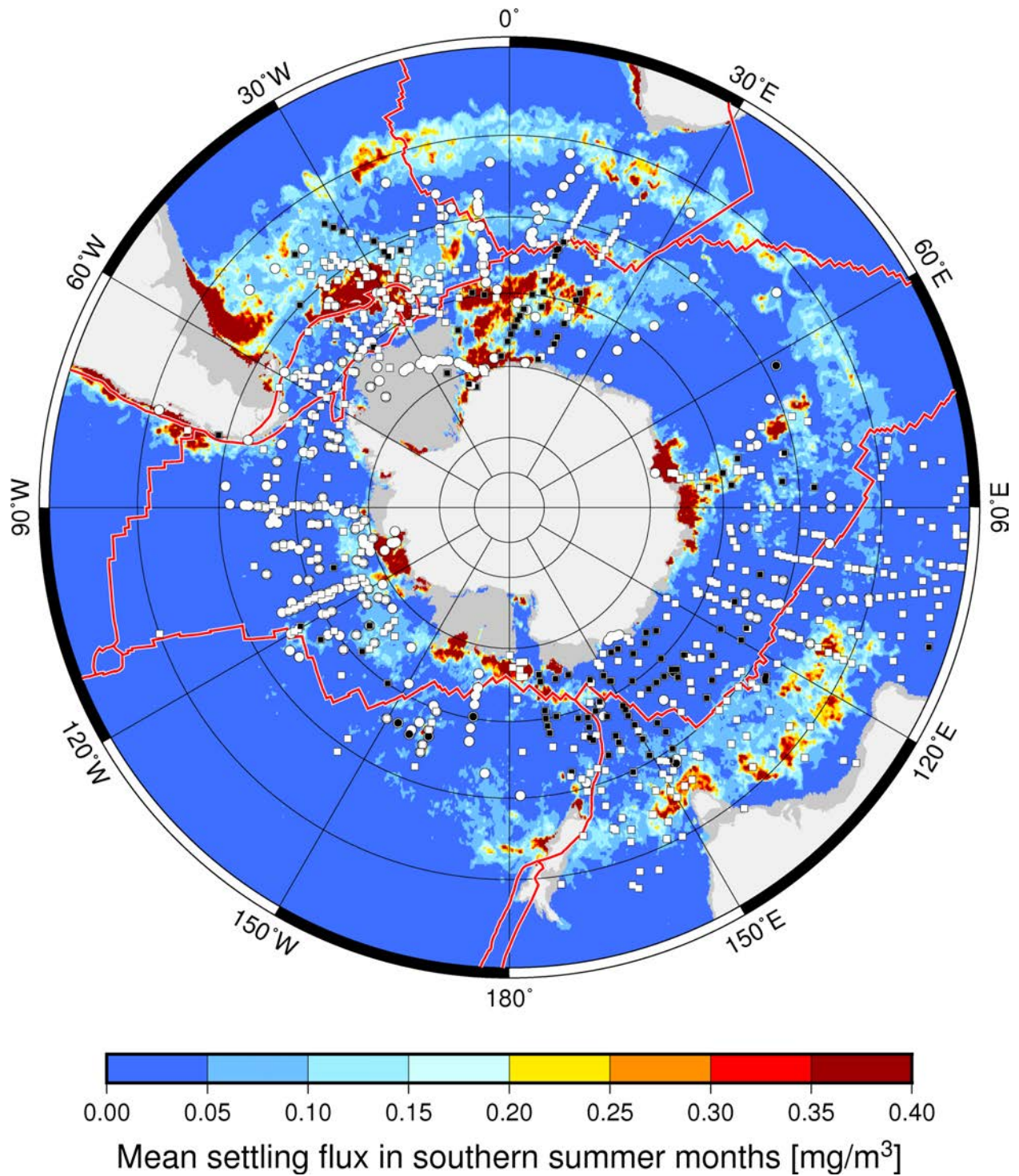


Figure DR17. Austral summer average of diatom chlorophyll concentrations for the period 2003-2013 (Soppa et al., 2014) overlain by conformities (white squares and white circles) and unconformities (black squares and black circles) in surface sediment of Bruhnes age (see Fig. DR7 caption for detail). Red lines with white outlines denote plate boundaries. Stereographic projection.

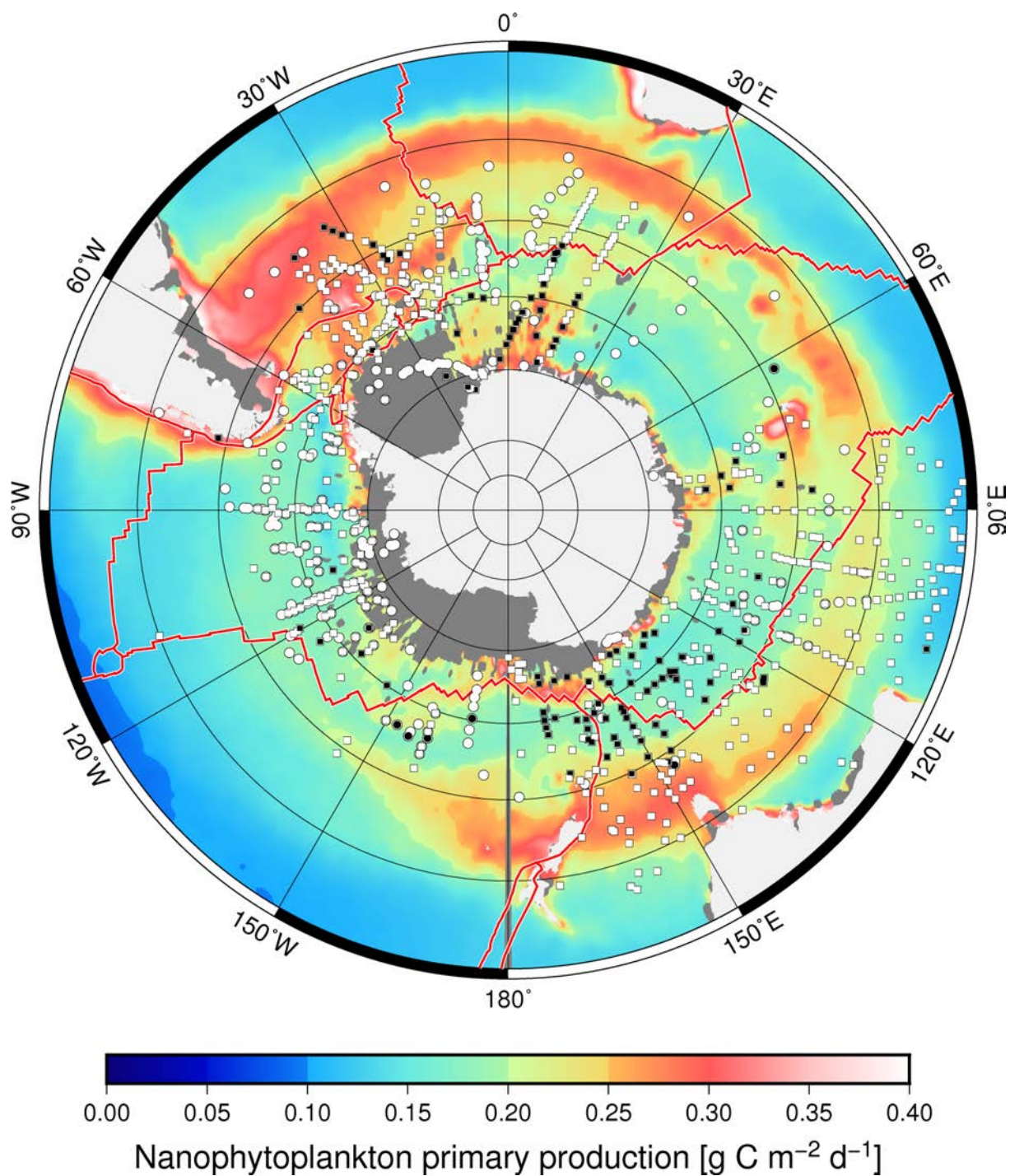


Figure DR18. Austral summer average of nanophytoplankton primary production for the period 1998-2007 (Uitz et al., 2010) overlain by conformities (white squares and white circles) and unconformities (black squares and black circles) in surface sediment of Bruhnes age (see Fig. DR7 caption for detail). Red lines with white outlines denote plate boundaries. Stereographic projection.

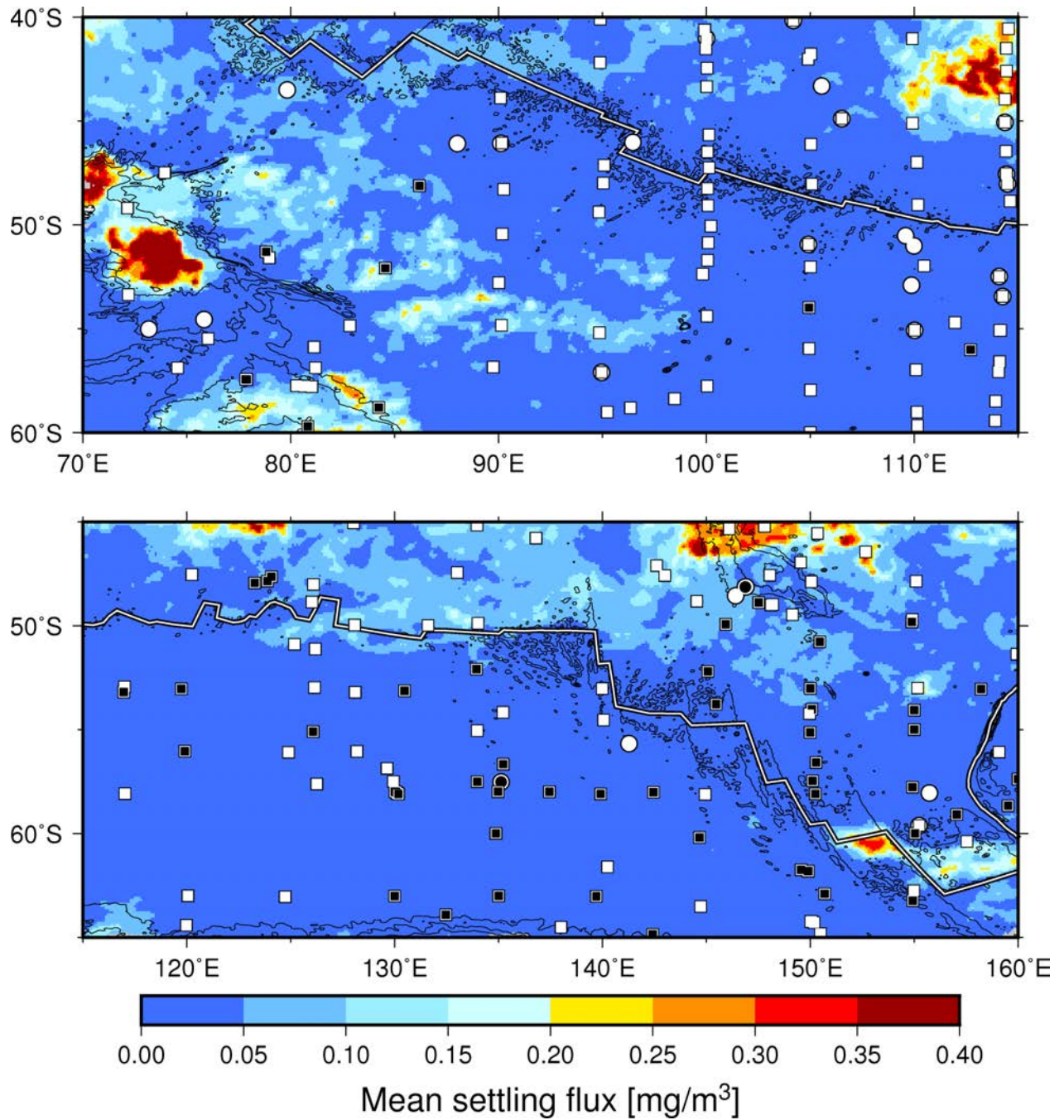


Figure DR19. Austral summer average of diatom chlorophyll concentrations for the period 2003-2013 (Soppa et al., 2014) overlain by conformities (white squares and white circles) and unconformities (black squares and black circles) in surface sediment of Bruhnes age (see Fig. DR7 caption for detail). Black-white lines denote plate boundaries. Equidistant cylindrical projection.

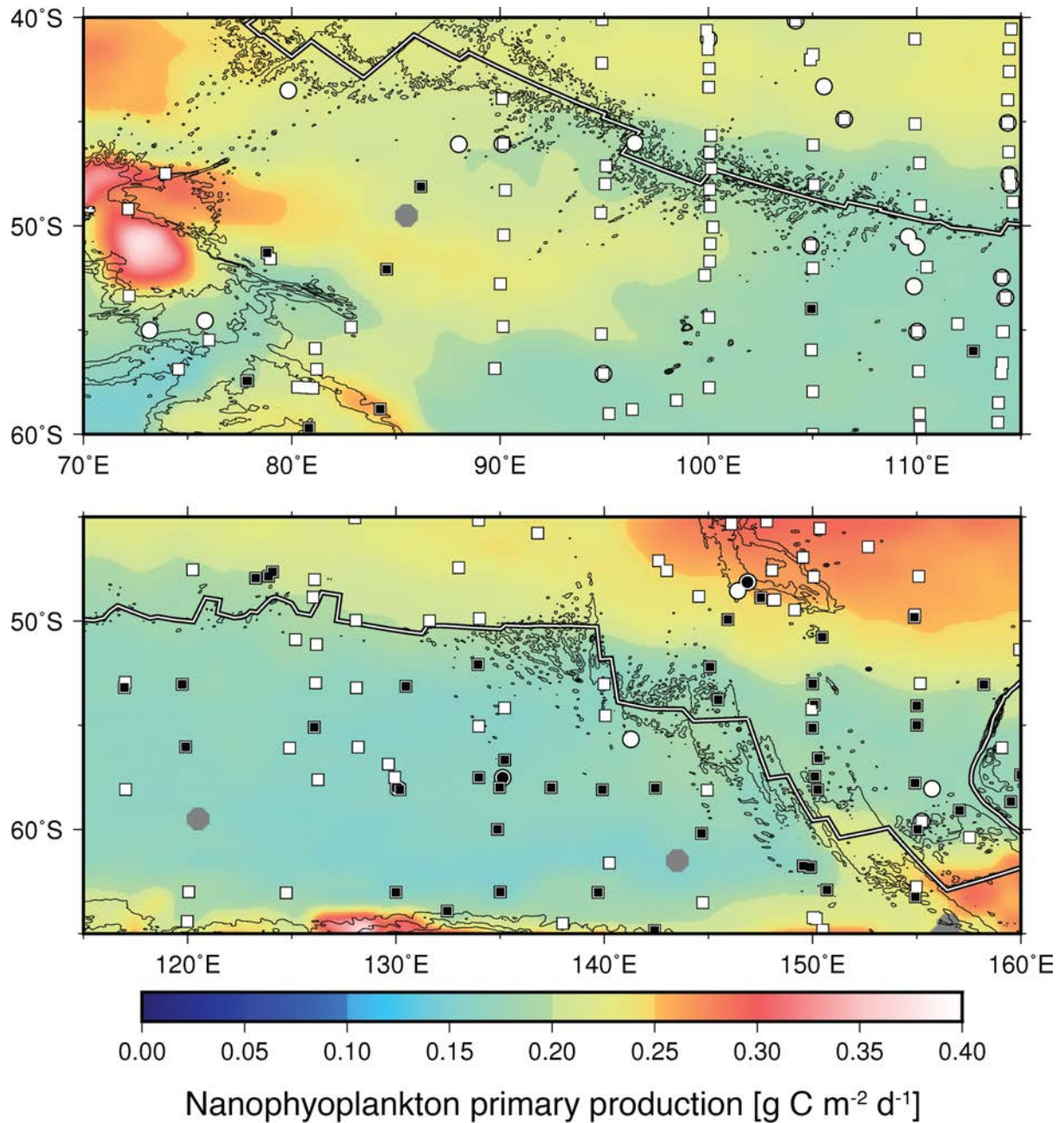


Figure DR20. Austral summer average of nanophytoplankton primary production for the period 1998-2007 (Uitz et al., 2010) overlain by conformities (white squares and white circles) and unconformities (black squares and black circles) in surface sediment of Brunhes age (see Fig. DR7 caption for detail). Red lines denote mid-ocean ridges. Gray circles are artefacts in the productivity grid. Black-white lines indicate plate boundaries. Equidistant cylindrical projection.

References:

- Allen, C. S., Pike, J., Pudsey, C. J., and Leventer, A., 2005a, Submillennial variations in ocean conditions during deglaciation based on diatom assemblages from the southwest Atlantic: *Paleoceanography*, v. 20, no. 2, p. PA2012,
- , 2005b, (Table 1) Age determination of sediment core KC073, 10.1594/PANGAEA.837085.
- Amante, C., and Eakins, B. W., 2009, ETOPO1 1 Arc-Minute Global Relief Model: Procedures, Data Sources and Analysis, National Geophysical Data Center, NOAA, NOAA Technical Memorandum NESDIS NGDC-24, NOAA Technical Memorandum NESDIS NGDC-24.
- Archer, D. E., 1996, An atlas of the distribution of calcium carbonate in sediments of the deep sea: *Global Biogeochemical Cycles*, v. 10, no. 1, p. 159-174,
- Archer, D. E., 1999, Opal, quartz and calcium carbonate content in surface sediments of the ocean floor, 10.1594/PANGAEA.56017.
- Bianchi, C., and Gersonde, R., 2004a, (Appendix Table 1) Age determination of sediment core PS1654-2, 10.1594/PANGAEA.712951.
- Bianchi, C., and Gersonde, R., 2004b, (Appendix Table 1) Age determination of sediment core PS2090-1, 10.1594/PANGAEA.712952.
- Bianchi, C., and Gersonde, R., 2004c, Climate evolution at the last deglaciation: the role of the Southern Ocean: *Earth and Planetary Science Letters*, v. 228, no. 3, p. 407-424,
- Bohrmann, G., 1999, Geochemistry of surface sediments from the South Atlantic, 10.1594/PANGAEA.54956.
- Bonn, W. J., Gingele, F. X., Grobe, H., Mackensen, A., and Fütterer, D. K., 1998a, Age model of sediment core PS1575-1, 10.1594/PANGAEA.50562.
- , 1998b, Age model of sediment core PS1821-6, 10.1594/PANGAEA.351294.
- , 1998c, Age model of sediment core PS2038-2, 10.1594/PANGAEA.351295.
- , 1998d, Palaeoproductivity at the Antarctic continental margin: opal and barium records for the last 400 ka: *Palaeogeography, Palaeoclimatology, Palaeoecology*, v. 139, no. 3, p. 195-211,
- Bradtmiller, L. I., Anderson, R. F., Fleisher, M. Q., and Burckle, L. H., 2009, Comparing glacial and Holocene opal fluxes in the Pacific sector of the Southern Ocean: *Paleoceanography*, v. 24, no. 2,
- Charles, C. D., and Fairbanks, R. G., 1992a, Evidence from Southern Ocean sediments for the effect of North Atlantic deep-water flux on climate: *Nature*, v. 355, p. 416-419,
- Charles, C. D., and Fairbanks, R. G., 1992b, (Table 1) Age determination of sediment core RC11-83., 10.1594/PANGAEA.726261.
- Chase, Z., Anderson, R. F., Fleisher, M. Q., and Kubik, P. W., 2003, Accumulation of biogenic and lithogenic material in the Pacific sector of the Southern Ocean during the past 40,000 years: *Deep Sea Research Part II: Topical Studies in Oceanography*, v. 50, no. 3, p. 799-832, doi:10.1016/S0967-0645(02)00595-7.
- Chase, Z., and Burckle, L. H., 2015, Compilation of ²³⁰Th-normalized opal burial and opal concentrations from Southern Ocean surface sediments, 10.1594/PANGAEA.846117.
- Chase, Z., Kohfeld, K. E., and Matsumoto, K., 2015, Controls on biogenic silica burial in the Southern Ocean: *Global Biogeochemical Cycles*, v. 29, no. 10, p. 1599-1616, doi: 10.1002/2015GB005186.

- Dezileau, L., Bareille, G., Reyss, J. L., and Lemoine, F., 2000, Evidence for strong sediment redistribution by bottom currents along the southeast Indian ridge: Deep Sea Research Part I: Oceanographic Research Papers, v. 47, no. 10, p. 1899-1936, doi:10.1016/S0967-0637(00)00008-X.
- Divins, D. L., 2004, Total Sediment Thickness of the World's Oceans and Marginal Seas, Domack, E. W., Jull, A. J. T., and Nakao, S., 1991a, Advance of East Antarctic outlet glaciers during the Hypsithermal: implications for the volume state of the Antarctic ice sheet under global warming: *Geology*, v. 19, no. 11, p. 1059-1062,
- , 1991b, (Table 1) Age determinations on ODP Hole 119-740A, 10.1594/PANGAEA.389054.
- , 1991c, (Table 1) Age determinations on sediment core Core302, 10.1594/PANGAEA.389055.
- , 1991d, (Table 1) Age determinations on sediment core DF79.009-GB, 10.1594/PANGAEA.389056.
- , 1991e, (Table 1) Age determinations on sediment core DF79.012-GB, 10.1594/PANGAEA.389057.
- Dutkiewicz, A., Müller, R. D., O'Callaghan, S., and Jónasson, H., 2015, Census of seafloor sediments in the world's ocean: *Geology*, v. 43, no. 9, p. 795-798,
- Francois, R., Bacon, M. P., Altabet, M. A., and Labeyrie, L. D., 1993, Glacial/interglacial changes in sediment rain rate in the SW Indian sector of Subantarctic waters as recorded by ^{230}Th , ^{231}Pa , U, and $\delta^{15}\text{N}$: *Paleoceanography*, v. 8, no. 5, p. 611-629,
- Francois, R., Frank, M., Rutgers van der Loeff, M. M., and Bacon, M. P., 2004, ^{230}Th normalization: An essential tool for interpreting sedimentary fluxes during the late Quaternary: *Paleoceanography*, v. 19, no. 1, p. 1-16,
- Frank, M., 2002a, Age model of sediment core PS1754-1, doi:10.1594/PANGAEA.81109.
- , 2002b, Age model of sediment core PS1772-8, doi:10.1594/PANGAEA.81108.
- Frank, M., Gersonde, R., and Mangini, A., 1999, Sediment redistribution, $^{230}\text{Th}_{\text{ex}}$ -normalization and implications for the reconstruction of particle flux and export paleoproductivity, in Fischer, G., and Wefer, G., eds., *Use of Proxies in Paleoclimatology: Examples from the South Atlantic*: Berlin Heidelberg, Springer-Verlag, p. 409-426.
- Frank, M., and Mackensen, A., 2002a, Age model of sediment core PS1756-5, doi:10.1594/PANGAEA.81106.
- Frank, M., and Mackensen, A., 2002b, Age model of sediment core PS2082-1, doi:10.1594/PANGAEA.81103.
- Froelich, P. N., Malone, P. N., Hodell, D. A., Ciesielski, P. F., Warnke, D. A., Westall, F., Hailwood, E. A., Nobes, D. C., Fenner, J., and Mienert, J., Biogenic opal and carbonate accumulation rates in the subantarctic South Atlantic: the late Neogene of Meteor Rise Site 704, in *Proceedings Proc. Ocean Drill. Program Sci. Results 1991*, Volume 114, p. 515-550.
- Geibert, W., Rutgers van der Loeff, M. M., Usbeck, R., Gersonde, R., Kuhn, G., and Seeberg - Elverfeldt, J., 2005, Quantifying the opal belt in the Atlantic and southeast Pacific sector of the Southern Ocean by means of ^{230}Th normalization: *Global Biogeochemical Cycles*, v. 19, no. 4, p. 1-13, doi: 10.1029/2005GB002465.
- Goodell, H. G., and Watkins, N. D., 1968, The paleomagnetic stratigraphy of the Southern Ocean: 20° West to 160° East longitude: *Deep Sea Research and Oceanographic Abstracts*, v. 15, p. 89-112, doi:10.1016/0011-7471(68)90030-2.

- Gozhik, P. F., Orlovsky, G. N., Mitin, L. I., Pavlov, A. Y., Rud, L. M., Yanchuk, E. A., Ivanik, M. M., Vodopyan, N. S., and Krasnozhina, Z. V., 1991a, *Geologiya i Metallogeniya Yuzhnogo Okeana (Geology and Metallogeny of the Southern Ocean)*, in Shnyukov, E. F., ed., Naukova Dumka (Kiev): in Russian, p. 192.
- , 1991b, (Table 13) Radiocarbon age of bottom sediments from the Southern Ocean, 10.1594/PANGAEA.782426.
- Grobe, H., and Mackensen, A., 1992a, Age model of sediment core PS1380-3, 10.1594/PANGAEA.50558.
- , 1992b, Late Quaternary climatic cycles as recorded in sediments from the Antarctic continental margin, in Kennett, J. P., and Warnke, D. A., eds., *The Antarctic Paleoenvironment: a perspective on Global Change*, Antarctic Research Series, American Geophysical Union.
- Howard, W. R., and Prell, W. L., 1994a, Age model of sediment core MD84-529, 10.1594/PANGAEA.263948.
- , 1994b, Age model of sediment core RC13-229, 10.1594/PANGAEA.52655.
- Howard, W. R., and Prell, W. L., 1994c, Late Quaternary CaCO₃ production and preservation in the Southern Ocean: Implications for oceanic and atmospheric carbon cycling: *Paleoceanography*, v. 9, no. 3, p. 453-482,
- Jacot Des Combes, H., Esper, O., De La Rocha, C. L., Abelmann, A., Gersonde, R., Yam, R., and Shemesh, A., 2008a, Diatom $\delta^{13}\text{C}$, $\delta^{15}\text{N}$, and C/N since the Last Glacial Maximum in the Southern Ocean: Potential impact of species composition: *Paleoceanography*, v. 23, no. 4, p. PA4209,
- , 2008b, (Table 1) Age determination of sediment cores from the Southern Ocean, Kennett, J. P., and Watkins, N. D., 1976, Regional deep-sea dynamic processes recorded by late Cenozoic sediments of the southeastern Indian Ocean: *Geological Society of America Bulletin*, v. 87, no. 3, p. 321-339, doi: 10.1130/0016-7606(1976)87<321:RDDPRB>2.0.CO;2.
- Kirshner, A. E., Anderson, J. B., Jakobsson, M., O'Regan, M., Majewski, W., and Nitsche, F. O., 2012a, Post-LGM deglaciation in Pine island Bay, west Antarctica: *Quaternary Science Reviews*, v. 38, p. 11-26,
- , 2012b, (Table 1) Radiocarbon ages of sediment cores obtained during Icebreaker Oden cruise OSO0910, Pine Island Bay, 10.1594/PANGAEA.812067.
- Labeyrie, L., Labracherie, M., Gorfti, N., Pichon, J. J., Vautravers, M., Arnold, M., Duplessy, J. C., Paterne, M., Michel, E., and Duprat, J., 1996a, Hydrographic changes of the Southern Ocean (southeast Indian sector) over the last 230 kyr: *Paleoceanography*, v. 11, no. 1, p. 57-76,
- , 1996b, (Table 3) Age determination of sediment core MD88-770, 10.1594/PANGAEA.52730.
- Labracherie, M., Labeyrie, L. D., Duprat, J., Bard, E., Arnold, M., Pichon, J.-J., and Duplessy, J.-C., (Table 4) Age determinations on sediment core MD84-527, 10.1594/PANGAEA.358352.
- , 1989a, Age determinations on sediment core MD73-025, 10.1594/PANGAEA.358348.
- , 1989b, (Table 4) Age determinations on sediment core MD84-551, 10.1594/PANGAEA.358353.
- Labracherie, M., Labeyrie, L. D., Duprat, J., Bard, E., Arnold, M., Pichon, J. J., and Duplessy, J. C., 1989c, The last deglaciation in the Southern Ocean: *Paleoceanography*, v. 4, no. 6, p. 629-638,
- Lamy, F., Arz, H. W., Kilian, R., Lange, C. B., Lembke-Jene, L., Wengler, M., Kaiser, J., Baeza-Urrea, O., Hall, I. R., and Harada, N., 2015a, Glacial reduction and millennial-scale

- variations in Drake Passage throughflow: Proceedings of the National Academy of Sciences, v. 112, no. 44, p. 13496-13501,
- , 2015b, (Table S1) Age model of sediment core 202-1233, 10.1594/PANGAEA.848126.
- , 2015c, (Table S1) Age model of sediment core MD07-3128, 10.1594/PANGAEA.848127.
- , 2015d, (Table S1) Age model of sediment core MR0806-PC09, 10.1594/PANGAEA.848128.
- Lamy, F., Gersonde, R., Winckler, G., Esper, O., Jaeschke, A., Kuhn, G., Ullermann, J., Martínez-García, A., Lambert, F., and Kilian, R., 2014a, Age control points of sediment core PS75/056-1, 10.1594/PANGAEA.826579.
- , 2014b, Age control points of sediment core PS75/059-2, 10.1594/PANGAEA.826580.
- , 2014c, Age control points of sediment core PS75/074-3, 10.1594/PANGAEA.826581.
- , 2014d, Age control points of sediment core PS75/076-2, 10.1594/PANGAEA.826582.
- , 2014e, Age control points of sediment core PS75/079-2, 10.1594/PANGAEA.826583.
- , 2014f, Age control points of sediment core PS75/083-1, 10.1594/PANGAEA.826584.
- , 2014g, Increased dust deposition in the Pacific Southern Ocean during glacial periods: Science, v. 343, no. 6169, p. 403-407,
- Ledbetter, M. T., and Ciesielski, P. F., 1986, Post-Miocene disconformities and paleoceanography in the Atlantic sector of the Southern Ocean: Palaeogeography, Palaeoclimatology, Palaeoecology, v. 52, no. 3, p. 185-214, doi:10.1016/0031-0182(86)90046-5.
- Mackensen, A., 1996, Age model of sediment core PS1768-8, doi:10.1594/PANGAEA.50559.
- Mackensen, A., Grobe, H., Hubberten, H.-W., and Kuhn, G., 1994a, Age model of sediment core PS1506-1, 10.1594/PANGAEA.50166.
- , 1994b, Age model of sediment core PS2082-1, 10.1594/PANGAEA.50167.
- , 1994c, Benthic foraminiferal assemblages and the $\delta^{13}\text{C}$ -signal in the Atlantic sector of the Southern Ocean: glacial-to-interglacial contrasts, in Zahn, R., Pederson, T. F., Kaminiski, M. A., and Labeyrie, L., eds., Carbon Cycling in the Glacial Ocean: Constraints on the Ocean's Role in Global Change, Volume NATO ASI Series I17: Berlin, Heidelberg, Springer-Verlag, p. 105-144.
- Mackensen, A., Rudolph, M., and Kuhn, G., 2001a, Age model of sediment core PS2498-1, doi:10.1594/PANGAEA.80801.
- , 2001b, (Table 2c) Age, TOC, primary production, and isotopes (*Cibicides* spp.) of sediment core PS2499-5, doi:10.1594/PANGAEA.65927.
- Maddison, E. J., Pike, J., and Dunbar, R., 2012a, Seasonally laminated diatom-rich sediments from Dumont d'Urville Trough, East Antarctic Margin: Late-Holocene Neoglacial sea-ice conditions: The Holocene, v. 22, no. 8, p. 857-875,
- , 2012b, (Table 1) Radiocarbon ages for sediment cores MD03-2597, NBP01-01-JPC17B and NBP01-01-KC17B, 10.1177/0959683611434223.
- Müller, R. D., Seton, M., Zahirovic, S., Williams, S. E., Matthews, K. J., Wright, N. M., Shephard, G. E., Maloney, K. T., Barnett-Moore, N., Hosseinpour, M., Bower, D. J., and Cannon, J., 2016, Ocean basin evolution and global-scale plate reorganization events since Pangea breakup: Annual Review of Earth and Planetary Sciences, v. 44, p. 107-138, 10.1146/annurev-earth-060115-012211.
- Murayama, M., Nakamura, T., and Taira, A., 2000a, (Table 2) Age determination of sediment cores from the Tasman Plateau, 10.1594/PANGAEA.855345.

- , 2000b, Variations of terrestrial input and marine productivity in the Southern Ocean (48°S) during the last two deglaciations: *Paleoceanography*, v. 15, no. 2, p. 170-180,
- Osborn, N. I., Ciesielski, P. F., and Ledbetter, M. T., 1983, Disconformities and paleoceanography in the southeast Indian Ocean during the past 5.4 million years: *Geological Society of America Bulletin*, v. 94, no. 11, p. 1345-1358, doi: 10.1130/0016-7606(1983)94<1345:DAPITS>2.0.CO;2
- Rebesco, M., Hernández-Molina, F. J., Van Rooij, D., and Wåhlin, A., 2014, Contourites and associated sediments controlled by deep-water circulation processes: state-of-the-art and future considerations: *Marine Geology*, v. 352, p. 111-154, doi:10.1016/j.margeo.2014.03.011.
- Rosenthal, Y., Boyle, E. A., Labeyrie, L., and Oppo, D., 1995a, Glacial enrichments of authigenic Cd and U in Subantarctic sediments: A climatic control on the elements' oceanic budget?: *Paleoceanography*, v. 10, no. 3, p. 395-413,
- , 1995b, (Table 3) Sedimentation rate versus age in core MD80-304, 10.1594/PANGAEA.388560.
- , 1995c, (Table 3) Sedimentation rate versus age in core MD88-769., 10.1594/PANGAEA.388561.
- , 1995d, (Table 3) Sedimentation rate versus age in core RC13-229, 10.1594/PANGAEA.388562.
- Shemesh, A., Hodell, D., Crosta, X., Kanfoush, S., Charles, C., and Guilderson, T., 2002a, Age-depth relation in sediment core TTN057-13-PC4, 10.1594/PANGAEA.842939.
- , 2002b, Sequence of events during the last deglaciation in Southern Ocean sediments and Antarctic ice cores: *Paleoceanography*, v. 17, no. 4, p. 8-1-8-7
- Skinner, L. C., Fallon, S., Waelbroeck, C., Michel, E., and Barker, S., 2010a, (Table S1) Age determination of sediment core MD07-3076, planktonic foraminifera., 10.1594/PANGAEA.829756.
- , 2010b, Ventilation of the deep Southern Ocean and deglacial CO₂ rise: *Science*, v. 328, no. 5982, p. 1147-1151,
- Soppa, M. A., Hirata, T., Silva, B., Dinter, T., Peeken, I., Wiegmann, S., and Bracher, A., 2014, Global retrieval of diatom abundance based on phytoplankton pigments and satellite data: *Remote Sensing*, v. 6, no. 10, p. 10,089-010,106, doi: 10.3390/rs61010089.
- Suman, D. O., and Bacon, M. P., 1989, Variations in Holocene sedimentation in the North American Basin determined from ²³⁰Th measurements: *Deep Sea Research Part A. Oceanographic Research Papers*, v. 36, no. 6, p. 869-878, 10.1016/0198-0149(89)90033-2.
- Uitz, J., Claustre, H., Gentili, B., and Stramski, D., 2010, Phytoplankton class - specific primary production in the world's oceans: seasonal and interannual variability from satellite observations: *Global Biogeochemical Cycles*, v. 24, no. 3, 10.1029/2009GB003680.
- Watkins, N. D., and Kennett, J. P., 1972, Regional sedimentary disconformities and Upper Cenozoic changes in bottom water velocities between Australasia and Antarctica: *Antarctica Oceanology II: The Australian-New Zealand Sector*, p. 273-293, doi: 10.1029/AR019p0273.
- Yu, E.-F., 1994, Variations in the Particulate Flux of ²³⁰Th and ²³¹Pa and Paleoceanographic Applications of the ²³¹Pa/²³⁰Th Ratio: *Massachusetts Institute of Technology*, 269 p.

